

FINDING TRANSITION PATHWAYS ON MANIFOLDS*

TIEJUN LI[†], XIAOGUANG LI[†], AND XIANG ZHOU[‡]

Abstract. When a randomly perturbed dynamical system is subject to some constraints, the trajectories of the system and the noise-induced most probable transition pathways are restricted on the manifold associated with the given constraints. We present a constrained minimum action method to compute the optimal transition pathways on manifolds. By formulating the constrained stochastic dynamics in a Stratonovich stochastic differential equation of the projection form, we consider the system as embedded in the Euclidean space and present the Freidlin–Wentzell action functional via large deviation theory. We then reformulate it as a minimization problem in the space of curves through Maupertuis principle. Furthermore we show that the action functionals are intrinsically defined on the manifold. The constrained minimum action method is proposed to compute the minimum action path with the assistance of the constrained optimization scheme. The examples of conformational transition paths for both single and double rod molecules in polymeric fluid are numerically investigated.

Key words. rare event, large deviation, optimal transition pathways, constrained stochastic dynamics

AMS subject classification. 65K10

DOI. 10.1137/140957780

1. Introduction. A large number of interesting behaviors of randomly perturbed dynamical systems are closely related to rare but important transition events between metastable states. Such rare events play a major role in chemical reactions, conformational changes of biomolecules, nucleation events, and the like. Theoretical understanding of such transition events and transition paths has attracted a lot of attentions for many years [13, 9]. The classic model is the following Ito stochastic differential equation (SDE) in \mathbb{R}^n with small noise amplitude:

$$(1.1) \quad dX_t = b(X_t) dt + \sqrt{\varepsilon} \sigma(X_t) dW_t.$$

In (1.1), the solution X_t is \mathbb{R}^n -valued, b is a vector field $\mathbb{R}^n \rightarrow \mathbb{R}^n$, σ is a matrix-valued function $\mathbb{R}^n \rightarrow \mathbb{R}^{n \times m}$, and W is an m -dimensional standard Brownian motion. The drift term $b(x)$ could be the gradient of a potential energy function or have a rather general form. The diffusion matrix $\sigma(x)$ is assumed uniformly nondegenerate. b and σ satisfy the regular smoothness conditions such as the global Lipschitz continuity and boundedness conditions.

According to the large deviation principle (LDP) developed by Freidlin and Wentzell [9], in the asymptotic regime of vanishing noise $\varepsilon \downarrow 0$, the most probable transition pathway in the time period $[0, T]$ between metastable states can be de-

*Received by the editors February 19, 2014; accepted for publication (in revised form) November 10, 2015; published electronically January 26, 2016.

<http://www.siam.org/journals/mms/14-1/95778.html>

[†]LMAM and School of Mathematical Sciences, Peking University, Beijing 100871, China (tieli@pku.edu.cn, lxg1023@pku.edu.cn). The first author was supported by NSFC under grants 11421101, 11171009 and 91130005 and by the National Science Foundation for Excellent Young Scholars (grant 11222114).

[‡]Department of Mathematics, City University of Hong Kong, Kowloon, Hong Kong SAR, China (xiang.zhou@cityu.edu.hk). The work of this author was supported by the Hong Kong GRF (109113, 11304314, 11304715).

scribed through the minimizer of the Freidlin–Wentzell action functional,

$$(1.2) \quad S_T[\phi] = \frac{1}{2} \int_0^T \|\sigma^{-1}(\phi)(\dot{\phi} - b(\phi))\|_2^2 dt,$$

for a nondegenerate square matrix σ . Based on this principle of least action, some numerical methods, such as the minimum action method and its adaptive version [8, 25], have been proposed and developed for a fixed time interval $[0, T]$ of interest. Another different formulation of the Freidlin–Wentzell theory, based on the Maupertuis principle [14], is the geometric minimum action method (gMAM) on the space of curves [10]. The path given by the gMAM can be viewed as the minimum action path of the original Freidlin–Wentzell action for an optimal T . In the special case that $b(x) = -\nabla V(x)$ and $\sigma(x) \equiv I$, where V is a potential function and I is the identity matrix, the minimum action path is a minimum energy path and the string method [7] is applicable to identify this path.

In practical applications, the dynamics of the system of concern may be subject to one or more constraints, such as the constant length of rigid molecules [5], the conservation of mass [24, 15], or more general constraints [4]. These constraints restrict the system to live in a particular manifold $\mathcal{M} \subset \mathbb{R}^n$, determined by all the constraints. Even when the stochastic perturbation is applied, the resulting stochastic system still has to satisfy these physical constraints. Based upon this consideration, it is natural and interesting to investigate the rare events occurring on manifolds. The following problems are fundamental to address in the first step. What is the suitable mathematical setup for the rare event study on manifolds? How to characterize the most probable transition path? If one embeds the considered stochastic dynamics on a manifold in the ambient space, does the resulting formulation depend on the choice of embedding? How to design the effective path-finding algorithm with the obtained results? The aim of this paper is to answer these questions and present some preliminary numerical studies for some simple models.

We first outline our methodology and major points of this paper. There is an intrinsic formulation of the SDE on a Riemannian manifold, and one could “translate” the classic Freidlin–Wentzell LDP in Euclidean space to this manifold case; however, the abstractness of this formulation hinders its practicability. We actually start from a stochastic system in \mathbb{R}^n with drift b and diffusion σ subject to independent (deterministic) constraints $\{c_k(x) = 0\}$ through Lagrange multipliers. By explicitly solving these Lagrange multipliers in the stochastic version, we derive an SDE in the ambient space but in the projection form, which elucidates the connection between the constrained SDE form and the projection form. This connection is a generalization of similar results studied in [4], but with a more transparent proof. With this connection, we obtain an SDE described by the projected drift Πb and the *degenerate* diffusion $\Pi\sigma$ for a projection operator Π from \mathbb{R}^n to the tangent bundle. And this SDE indeed lives on the manifold with the unique drift $\tilde{b} = \Pi b$ and the diffusion $\tilde{\sigma} = \Pi\sigma$. By using the generalization of the Freidlin–Wentzell LDP in the degenerated diffusion case, we derive the specific forms of action functionals by introducing the generalized inverse of the projection operator Π . Moreover, we prove that our results of the action functionals depend only on Πb and $\Pi\sigma$, not on their extensions and the embedding in \mathbb{R}^n . We also derive the geometric formulation of the action functional on the space of curves and the Euler–Lagrange equation that the minimizing path must satisfy. We find that in the gradient case, i.e., $b = -\nabla V$ and $\sigma = I$, the projection-type string method works [6], while in general cases, the direct application

of existing pathway finding approaches with projection does not apply. We instead propose our constrained gMAM in the ambient space. In a nutshell, we present the basic mathematical setup and investigate some essential ingredients for the study of rare events on manifolds, and we demonstrate a viable numerical approach to compute the optimal transition path.

The paper is organized as follows. We first discuss the SDE on manifolds and the abstract form of the Freidlin–Wentzell action functional in the corresponding setup in section 2. In section 3, we develop our model and discuss the variational characterization of transition paths and the issue of embeddings following the idea we mentioned above. Section 4 is devoted to the discussion of the numerical methods—the constrained minimum action method. The applications to liquid crystal models are presented in section 5, where we study the conformational transitions for rod molecules on \mathbb{S}^2 (unit sphere) and $\mathbb{S}^2 \times \mathbb{S}^2$. In section 6, we show some possible extensions to general bead-rod chain systems. The summary is in section 7. The detailed technical proofs and some discussion about the comparison of different action functionals are in the appendix.

2. SDE and LDP on manifolds. We first give an introduction to the formulation of describing the SDE on a Riemannian manifold and the formal extrapolation of the classic Freidlin–Wentzell theory for this manifold setting. The SDE on the manifold is most conveniently written in the Stratonovich sense [12],

$$(2.1) \quad dX_t = b(X_t) dt + \sqrt{\varepsilon} \sum_{k=1}^L \sigma_k(X_t) \circ dW_t^k,$$

on a compact differentiable d -dimensional manifold \mathcal{M} without boundary. Here $X \in \mathcal{M}$, the drift and diffusion $b(x)$ and $\sigma_k(x)$ belong to $T_x\mathcal{M}$ (the tangent space of \mathcal{M} at x) and $\{W^k\}_{k=1}^L$ are independent Wiener processes on \mathbb{R} . We assume the nondegenerate condition for diffusion,

$$\dim \text{span}\{\sigma_k(x)\}_{k=1}^L = d \quad \forall x \in \mathcal{M}.$$

For the Brownian motion on Riemannian manifold ($b = 0$ and σ is the orthogonal projection operator related to the Laplace–Beltrami operator; see, e.g., [12]), [11] proved the LDP for the short time limit and gave the rate function. The minimizing path of this rate function for the Brownian motion is the minimizing geodesics on the manifold from starting point to ending point. For the SDE case rather than Brownian motion, we here formally “extrapolate” the existing result on the Freidlin–Wentzell LDP in Euclidean \mathbb{R}^n to the manifold case. It will be shown later that we eventually work on the SDE in the ambient space and use the corresponding LDP for the Euclidean case.

Under certain regularity conditions on b and σ_k , we can write, as least in a formal way, the rate function (or action functional) for (2.1) when $\varepsilon \downarrow 0$ as

$$(2.2) \quad S_T[\phi] = \int_0^T L(\phi, \dot{\phi}) dt,$$

when $\phi \in AC([0, T]; \mathcal{M})$, AC meaning absolutely continuous functions. Otherwise, $S_T[\phi] = +\infty$. Here $\dot{\phi}$ is the time derivative $d\phi/dt$. The Lagrangian in (2.2) $L : \mathcal{M} \times T\mathcal{M} \rightarrow \mathbb{R}$ is defined as

$$(2.3) \quad L(x, y) := \frac{1}{2} \langle a^{-1}(y - b(x)), y - b(x) \rangle,$$

where $\langle \cdot, \cdot \rangle$ is the dual product between the cotangent space $T^*\mathcal{M}$ and the tangent space $T\mathcal{M}$. Equation (2.3) can be treated as $\frac{1}{2}\|y - b(x)\|_{\mathcal{M}}^2$, where the norm in $T\mathcal{M}$, $\|y\|_{\mathcal{M}} := \langle y, a^{-1}y \rangle$, is induced by the inverse of the nondegenerate $a(x) = \sigma(x) \otimes \sigma(x)$.

Remark 1. Note that the type $(0, 2)$ covariant symmetric tensor field

$$\sum_{k=1}^m \sigma_k \otimes \sigma_k \in T_0^2\mathcal{M}$$

can also be viewed as a mapping

$$a := \sum_{k=1}^m \sigma_k \otimes \sigma_k : T^*\mathcal{M} \longrightarrow T\mathcal{M}$$

by fixing its first or second argument [2]. From the nondegenerate condition, we have that the mapping a is bijective; thus its inverse $a^{-1} : T\mathcal{M} \rightarrow T^*\mathcal{M}$ is well-defined.

Remark 2. The classic Freidlin–Wentzell LDP is formulated for the Ito SDE. So, it appears that the action functional, (2.2) and (2.3), would only correspond to the SDE (2.1) interpreted in the Ito sense. Indeed, the LDP action functional, (2.2) and (2.3), still has exactly the same expression no matter whether (2.1) is in the Ito sense or the Stratonovich sense, because the LDP here is for the limit $\varepsilon \downarrow 0$. We use (1.1) in Euclidean space to elaborate this point. Consider the following SDE with the same form of drift and diffusion as the Ito (1.1), but in the Stratonovich sense:

$$(2.4) \quad dX_t = b(X_t) dt + \sqrt{\varepsilon}\sigma(X_t) \circ dW_t.$$

We know (2.4) is equivalent to the following Ito SDE:

$$(2.5) \quad dX_t = b^\varepsilon(X_t) dt + \sqrt{\varepsilon}\sigma(X_t) dW_t,$$

where $b_i^\varepsilon(x) = b_i(x) + \frac{\varepsilon}{2} \sum_{j=1}^n \sum_{k=1}^m \frac{\partial \sigma_{ik}(x)}{\partial x_j} \sigma_{jk}(x)$. By [9] or [3], if $b^\varepsilon \rightarrow b$ uniformly in the maximum norm as $\varepsilon \rightarrow 0$, for example, when σ and its derivative are uniformly bounded for the situation here, then the Ito SDE (2.5) (equivalently, the Stratonovich SDE (2.4)) and the Ito SDE (1.1) share the same large deviation result with the same rate function (1.2).

Therefore, under mild conditions, it is valid to take limit $\varepsilon \downarrow 0$ for the ε -dependent drift function first to have an ε -independent drift for the use of the action functional in the Freidlin–Wentzell LDP.

There is a conjugate relation between the Lagrangian and the Hamiltonian for the underlying LDP. The Hamiltonian corresponding to (2.3), $H : \mathcal{M} \times T^*\mathcal{M} \rightarrow \mathbb{R}$, has the following form:

$$H(x, p) := \langle p, b(x) \rangle + \frac{1}{2} \sum_{k=1}^m \langle p, \sigma_k(x) \rangle^2.$$

We show that (2.3) is indeed the Legendre transformation of the Hamiltonian, i.e.,

$$(2.6) \quad L(x, y) = \sup_{p \in T^*\mathcal{M}} \{ \langle p, y \rangle - H(x, p) \}.$$

To show this, we calculate the critical point of (2.6)

$$(2.7) \quad y = \frac{\partial H}{\partial p} = b(x) + \sum_{k=1}^m \langle p, \sigma_k(x) \rangle \sigma_k(x)$$

to get the optimal $p^*(x, y) = a^{-1}(y - b(x))$. Plugging this p^* into the right-hand side of (2.6), we immediately see that (2.6) holds. In addition, we have that $p^*(\phi, \dot{\phi})$ is equal to the generalized momentum defined as $\frac{\partial L}{\partial y}(\phi, \dot{\phi}) = a^{-1}(\dot{\phi} - b(\phi))$. We also have that along a path ϕ , $H(\phi, p^*(\phi, \dot{\phi})) = \frac{1}{2}\|\dot{\phi}\|_{\mathcal{M}}^2 - \frac{1}{2}\|b(\phi)\|_{\mathcal{M}}^2$.

The geometric action functional \hat{S} for the SDE (2.1) on the manifold \mathcal{M} can also be formally generalized as for the Euclidean case in [10] by using the Maupertuis principle (section 44 in [14]), which says that the geometric action (also called *abbreviated action*) is the following line integration of the generalized momentum along a curve $\gamma = \{\varphi(\alpha) : \alpha \in [0, 1]\}$ on \mathcal{M} :

$$\hat{S}[\varphi] = \int_{\gamma} \langle p^*, d\varphi \rangle$$

with the constraint $H(\gamma, p^*) \equiv 0$. In the case of (2.1) here, $p^* = a^{-1}(\dot{\phi} - b(\phi))$, where $\phi(t)$ is the t -parametrization of the curve γ . Write $\varphi' = \frac{d\varphi}{d\alpha}$. Note that $H(\gamma, p^*) \equiv 0$ gives that $\|\varphi'\|_{\mathcal{M}} \frac{d\alpha}{dt} = \|b(\varphi)\|_{\mathcal{M}}$. Thus, $p^* = a^{-1}(\varphi' \frac{d\alpha}{dt} - b(x)) = a^{-1}(\frac{\varphi'}{\|\varphi'\|_{\mathcal{M}}} \|b(\varphi)\|_{\mathcal{M}} - b(x))$. Thus, we have the geometric action functional for (2.1)

$$(2.8) \quad \hat{S}[\varphi] = \int_{\gamma} \langle a^{-1}(\tau(\varphi)\|b(\varphi)\|_{\mathcal{M}} - b(x)), d\varphi \rangle,$$

where $\tau = \varphi' / \|\varphi'\|_{\mathcal{M}}$ is the normalized tangent. It is clear that (2.8) is invariant for specific parametrization of the curve γ .

3. Action functional for constrained SDE. The abstract formulation in section 2 is intrinsically defined for a Riemannian manifold \mathcal{M} . However, for real applications, the SDE of interest is usually written in an ambient space, say, \mathbb{R}^n , subject to some constraints, such as the example of a polymer chain in section 6. Thus the resulting trajectories of the SDE lie in the submanifold immersed in \mathbb{R}^n . For the deterministic dynamics subjected to imposed constraints, one of the traditional approaches is to introduce the Lagrange multipliers. By explicitly solving the Lagrange multiplier from the constraints, one can obtain a new dynamical flow in ambient space, but naturally living on the submanifold determined by the constraints. This flow on the submanifold is equivalent to projecting the original flow onto the tangent space of the submanifold.

We shall take a similar approach to model the problem of the “constrained SDE” and show the equivalence of the Lagrange multiplier approach and the projection approach. The purpose here is to rigorously derive the correct form of the “projected SDE” embedded in the ambient space. After we derive this SDE in the projection form, we treat it as an SDE in the ambient space with degenerate diffusion, from which we carry out the study of the action functional in LDP.

3.1. Constrained SDE in ambient space. Consider a stochastic dynamics written as an Ito SDE in \mathbb{R}^n ,

$$(3.1) \quad dX = b(X) dt + \sigma(X) dW$$

subject to $p = n - d$ independent constraints $c_j(X) = 0, j = 1, \dots, p$.

To incorporate these constraints, we introduce the Lagrangian multipliers $\mu = (\mu_1, \dots, \mu_p)^\top$, as well as the Jacobian of the constraint functions

$$(3.2) \quad G(x) = \begin{pmatrix} (\nabla c_1(x))^\top \\ (\nabla c_2(x))^\top \\ \vdots \\ (\nabla c_p(x))^\top \end{pmatrix} \in \mathbb{R}^{p \times n} \quad \text{and} \quad M(x) = G(x)G^\top(x) \in \mathbb{R}^{p \times p}.$$

The matrix M can be considered as a metric matrix in the normal space spanned by $\{\nabla c_j(x)\}$. The independence of the constraints amounts to the condition that $M^{-1}(x)$ exists for any x . Now we consider the constrained SDE of the form

$$(3.3) \quad dX = b(X) dt + G^\top(X) d\mu + \sigma(X) dW,$$

where the Lagrange multiplier μ is described by

$$(3.4) \quad d\mu = \alpha(X) dt + \beta(X) dW.$$

The driving Brownian motion W in (3.3) and W in (3.4) are the same. The functions $\alpha(x) \in \mathbb{R}^p$ and $\beta(x) \in \mathbb{R}^{p \times n}$ above will be determined by the constraints such that the solution X_t to (3.3) and (3.4) satisfies $c_j(X_t) \equiv 0 \quad \forall j, \forall t \geq 0$ as long as $c_j(X_0) = 0$. The calculations by using the Ito lemma show the following result.

THEOREM 1. *The functions α and β in (3.4) for the Lagrange multipliers have the form*

$$(3.5) \quad \alpha = -M^{-1} \left[Gb + \frac{1}{2} \nabla^2 c : (BB^\top) \right]$$

and

$$(3.6) \quad \beta = -M^{-1} G\sigma,$$

where $B = G^\top \beta + \sigma$, and $(\nabla^2 c : (BB^\top))_i := \sum_{j,k,m=1}^n (\partial_{jk} c_i) B_{jm} B_{km}$.

If the primitive diffusion coefficient σ satisfies the condition that

$$(3.7) \quad a(x) := \sigma(x)\sigma(x)^\top = \theta(x)I,$$

where θ is a positive scalar, then (3.3) is equivalent to the Stratonovich SDE

$$(3.8) \quad dX = P(X) \left(b(X) dt + \sigma(X) \circ dW \right),$$

where

$$(3.9) \quad P = I - G^\top M^{-1} G$$

is the orthogonal projection onto the tangent space of the manifold arising from the constraints:

$$\mathcal{M} = \{x \in \mathbb{R}^n : c_j(x) = 0, j = 1, \dots, p\}.$$

The action of the projection operator P in (3.8) is understood in the Stratonovich sense.

If $a = \sigma\sigma^\top$ is not a scalar matrix, then the Stratonovich projection form (3.9) is generally not true. But for the vanishing noise limit, we still have the following result.

COROLLARY 1. *If the term $\sigma(x)$ in (3.3) is replaced by $\sqrt{\varepsilon}\sigma(x)$, then the constrained SDE (3.3), (3.4) can be transformed to*

$$(3.10) \quad dX = P(X) \left((b(X) + h(X, \varepsilon)) dt + \sqrt{\varepsilon}\sigma(X) \circ dW \right),$$

where $\|h(x, \varepsilon)\| \sim O(\varepsilon)$.

The proof of this corollary is straightforward by direct calculations using (3.5) and (3.6). The h term above actually comes from the F_1 term in the proof of Proposition 1. Since the action functional is unchanged if the term $h(x, \varepsilon)$ is taken out in (3.10), due to the same argument in Remark 2, we can use (3.8) to study the transition path problem, regardless of the condition (3.7). It should be noted that for finite noise, (3.8) and (3.10) are different SDEs, although they share the same rate function at the large deviation level.

3.2. SDE embedded in ambient space. We have shown the transformation of an Ito SDE in the ambient space subject to constraints into a projection form by introducing the orthogonal projection operator P . In comparison to the deterministic case, the Lagrange multiplier μ carries information of both the drift b and the diffusion σ . Therefore, the drift of the resulting SDE (3.10) has an additional term from the diffusion σ , except that $\sigma\sigma^\top$ is a scalar matrix. Since here we are interested only in the transition pathways of these SDEs and the large deviation rate functions are the same if the drift terms in these SDEs have only an order $O(\varepsilon)$ perturbation, we can study (3.10) by taking out the extra h term, which is the following projected SDE:

$$(3.11) \quad dX = P(X) (b(X) dt + \sqrt{\varepsilon}\sigma(X) \circ dW).$$

In what follows, we shall view this SDE in projection form as an extension in \mathbb{R}^n of the SDE intrinsically defined on manifold as in section 2.

Assume that a d -dimensional closed Riemannian submanifold \mathcal{M} is a submanifold in the ambient Euclidean space \mathbb{R}^n ($n > d$) by isometric embedding. The Riemannian metric on \mathcal{M} is naturally induced by Euclidean metric in \mathbb{R}^n . We consider the following Stratonovich SDE intrinsically defined on \mathcal{M} (see (2.4)):

$$(3.12) \quad dX = \tilde{b}(X) dt + \sqrt{\varepsilon} \sum_{k=1}^n \tilde{\sigma}_k(X) \circ dW_t^k,$$

where \tilde{b} and $\tilde{\sigma}_k, \mathcal{M} \rightarrow T\mathcal{M}$, are vector fields on \mathcal{M} and the driving Brownian motion $\{W^k : k = 1, \dots, n\}$ is the standard Brownian motion in \mathbb{R}^n . $\tilde{\sigma}(x) := [\tilde{\sigma}_1, \dots, \tilde{\sigma}_n]$ is a linear mapping $\mathbb{R}^n \rightarrow T_x\mathcal{M}$ for each $x \in \mathcal{M}$ and is assumed to be nondegenerate on \mathcal{M} ; that is,

$$\text{span}\{\tilde{\sigma}_k(x) : k = 1, \dots, n\} = T_x\mathcal{M} \quad \forall x \in \mathcal{M}.$$

Write $\tilde{a}(x) := \tilde{\sigma}(x)\tilde{\sigma}(x)^\top$. The nondegeneracy of $\tilde{\sigma}$ implies that $\tilde{a}(x)$ is positive definite and invertible as a linear mapping from $T_x^*\mathcal{M}$ to $T_x\mathcal{M}$.

A special case of (3.12) is the Brownian motion, in which, by [12, Thm. 3.1.4], $\tilde{b} = 0|_{\mathcal{M}}$ and $\tilde{\sigma}_k = P_k$, the orthogonal projection of the standard orthonormal basis

on \mathbb{R}^n onto the tangent bundle $T\mathcal{M}$. Let P be a corresponding orthogonal projection matrix from \mathbb{R}^n to $T\mathcal{M}$, i.e., $P(x) = [P_1(x), \dots, P_n(x)]$; then the solution of $dX = P(X) \circ dW := \sum_{k=1}^n P_k(X) \circ dW^k$ is the Brownian motion on \mathcal{M} .

Extending $\tilde{b}(x)$ and $\tilde{\sigma}_k(x)$ in (3.12) arbitrarily to the ambient space $x \in \mathbb{R}^n$, we can identify (3.12) on \mathcal{M} as the following extrinsic SDE on \mathbb{R}^n :

$$(3.13) \quad dX = \Pi \left(b(X) dt + \sqrt{\varepsilon} \sum_{k=1}^n \sigma_k(X) \circ dW_t^k \right),$$

where $\Pi = \Pi_x$ is a projection matrix (not necessarily orthogonal matrix) from \mathbb{R}^n to $T_x\mathcal{M}$. The tangent space $T_x\mathcal{M}$ is now identified as $\text{Img}(\Pi_x)$, a d -dim subspace of \mathbb{R}^n . The subindex of the projection Π is sometimes dropped out henceforth if there is no ambiguity. With probability 1, if the initial condition $X_0 = x \in \mathcal{M}$, the solution of (3.13) X_t is always on the manifold \mathcal{M} for any time $t > 0$.

By identifying \tilde{b} in (3.12) as a vector field on \mathbb{R}^n , we require that

$$\Pi(b(x)) = \tilde{b}(x) \quad \forall x \in \mathcal{M}.$$

Let $\sigma := [\sigma_1, \dots, \sigma_n]$. We assume that σ is nondegenerate in \mathbb{R}^n , i.e.,

$$\text{span} \{ \sigma_1, \dots, \sigma_n \} = \mathbb{R}^n.$$

Then we further require that

$$\Pi\sigma(x) = \tilde{\sigma}(x)$$

$\forall x$ on \mathcal{M} with the same range space $T_x\mathcal{M}$. When σ is the identity matrix in \mathbb{R}^n , the diffusion term is $\Pi \circ dW$, corresponding to the Brownian motion on \mathcal{M} .

Equation (3.13) is the same as (3.11) if the manifold \mathcal{M} is determined by the $p = n - d$ independent constraints; however, in (3.13) we do not assume that Π must be an orthogonal projection, although the results can be further simplified if Π is indeed orthogonal.

Next, we give some comments to emphasize that \tilde{a} indeed induces a metric on $\text{Img}(\Pi) = T_x\mathcal{M}$. Since $\tilde{a}(x) = \tilde{\sigma}(x)\tilde{\sigma}(x)^\top$ and $a(x) = \sigma(x)\sigma(x)^\top$, then

$$(3.14) \quad \tilde{a}(x) = \Pi a(x) \Pi^\top \quad \forall x \in \mathcal{M}.$$

Note that \tilde{a} is a linear mapping from \mathbb{R}^n to $\text{Img}(\Pi)$ with the same kernel space as $\tilde{\sigma}^\top$ and Π^\top . Thus, for any $v \in \text{Img}(\Pi)$, there is a unique vector \tilde{v} in $\text{Img}(\Pi)$ such that the linear equation $\tilde{a}\tilde{v} = v$ holds. For such a \tilde{v} , we have $v^\top\tilde{v} = \tilde{v}^\top\tilde{a}\tilde{v} \geq 0$ and the equality $\tilde{v}^\top\tilde{a}\tilde{v} = 0$ holds if and only if $\tilde{v} = 0$. Thus, we can define \tilde{a} -norm on the subspace $\text{Img}(\Pi)$ as follows:

$$(3.15) \quad \|v\|_{\tilde{a}} := \sqrt{\langle v, \tilde{v} \rangle} = \sqrt{v^\top\tilde{v}}.$$

Formally we can write $\tilde{v} = \tilde{a}^{-1}v$, then $\|v\|_{\tilde{a}} = \sqrt{\langle v, \tilde{a}^{-1}v \rangle}$. Here $\langle \cdot, \cdot \rangle$ is the Euclidean inner product of \mathbb{R}^n . Meanwhile, the \tilde{a} -inner product is also induced as $\langle w, v \rangle_{\tilde{a}} = \langle \tilde{a}^{-1}w, v \rangle = \langle w, \tilde{a}^{-1}v \rangle$. For the special case that $a(x) = I$ and $\Pi = \Pi^\top$ (orthogonal projection), $\tilde{a}v = \Pi v = v$ for any $v \in T_x\mathcal{M}$ and thus both \tilde{a} and \tilde{a}^{-1} are $I|_{T_x\mathcal{M}}$, the identity mapping restricted on $T_x\mathcal{M}$.

The vector field \tilde{b} and the diffusion tensor \tilde{a} uniquely define a unique SDE (3.12) on \mathcal{M} . We extended the domains of \tilde{b} and \tilde{a} to b and a , respectively, by introducing

the projection Π to have an equivalent SDE (3.13) embedded in the ambient space. By viewing this projection form SDE (3.13) as an \mathbb{R}^n -valued SDE in the ambient space, we can study its LDP and action functional. Obviously, the extended b , a and the choice of Π are not unique in the ambient space. Will the LDP result and the action functional obtained from the ambient space depend on the nonunique extensions of $b(x)$ and $a(x)$? We next show that the answer is no and the final result of the action functional of (3.13) depends only on the intrinsic flow \tilde{b} (i.e., Πb) and the \tilde{a} -norm on \mathcal{M} .

3.3. Action functional. Equation (3.13) on Euclidean \mathbb{R}^n has degenerate diffusion restricted in $T_x\mathcal{M}$, a subspace of \mathbb{R}^n . The classic Freidlin–Wentzell theory [9] for the nondegenerate case is not directly applicable. The Freidlin–Wentzell LDP result has been generalized for the degenerate case. Refer to [3, 1, 20] and the literature therein. Under certain mild assumptions for Πb and $\Pi\sigma$ (sublinear growth, locally Lipschitz continuity in \mathbb{R}^n , etc.), it follows from [3] that the LDP of the Freidlin–Wentzell estimate holds with the rate function given by

$$(3.16) \quad S[\phi] = \int_0^T L(\phi, \dot{\phi}) dt = \inf_{f \in L^2([0, T]; \mathbb{R}^n)} \left\{ \frac{1}{2} \int_0^T \|f\|^2 dt : \dot{\phi} - \Pi b(\phi) = \Pi\sigma f \right\}$$

if $\phi \in AC([0, T], \mathbb{R}^n)$ and $S[\phi] = +\infty$ otherwise. Here $\Pi = \Pi_{\phi(t)}$ and $\dot{\phi} = d\phi/dt$ is the time derivative. The norm $\|f\|$ is the 2-norm in \mathbb{R}^n . Equation (3.16) implies that for any path with finite action, its velocity $\dot{\phi}$ must lie in $\text{Img}(\Pi)$, which is just the tangent bundle $T\mathcal{M}$. Let the two ends of the path be fixed at two given points A and B on \mathcal{M} , i.e., $\phi(0) = A$ and $\phi(T) = B$. Then $\dot{\phi} \in T\mathcal{M}$ implies that the path with finite action must be in the admissible set

$$(3.17) \quad \mathcal{A} = \{ \phi \in AC([0, T]; \mathcal{M}) : \phi(0) = A, \phi(T) = B \},$$

which is equivalent to

$$(3.18) \quad \mathcal{A}' = \left\{ \phi \in AC([0, T]; \mathbb{R}^n) : \dot{\phi} \in \text{Img}\Pi_\phi, \phi(0) = A, \phi(T) = B \right\}.$$

The Lagrangian $L(x, y) : \mathcal{M} \times T\mathcal{M} \rightarrow \mathbb{R}$ in (3.16) has the following form by introducing $u = \sigma f(t)$ for each t :

$$(3.19) \quad L(x, y) = \min_{u \in \mathbb{R}^n, \Pi u = y - \Pi b(x)} \frac{1}{2} \|u\|_a^2.$$

Recall that $a(x) = \sigma(x)\sigma(x)^T$ is nondegenerate and positive definite in \mathbb{R}^n and $\|u\|_a := \sqrt{u^T a^{-1}(x)u}$ for $u \in \mathbb{R}^n$. So (3.19) is a quadratic programming and the solution u is unique in general. The following result relates the above minimization problem to the \tilde{a} -norm we defined before.

PROPOSITION 1. *For any vector $v \in T_x\mathcal{M}$, we have that*

$$(3.20) \quad \min_{u \in \mathbb{R}^n, \Pi u = v} \|u\|_a^2 = \|v\|_{\tilde{a}}^2,$$

where \tilde{a} is defined in (3.14) and $\|\cdot\|_{\tilde{a}}$ is defined in (3.15). In addition, the optimal $u^* = a\Pi^T \tilde{a}^{-1}v$. Furthermore, if $\Pi^T = \Pi$, then $u^* = a\tilde{a}^{-1}v$.

Proof. Write $\tilde{v} := \tilde{a}^{-1}v$. By the definition of \tilde{a} and \tilde{a}^{-1} , we have $\tilde{a}\tilde{v} = \Pi a \Pi^T \tilde{v} = v$. Introduce $l := u - a \Pi^T \tilde{v}$, then $\Pi l = 0$. We have that

$$\begin{aligned} \|u\|_a^2 &= u^T a^{-1} u = (l + a \Pi^T \tilde{v})^T (a^{-1} l + \Pi^T \tilde{v}) \\ &= \|l\|_a^2 + \tilde{v}^T \Pi l + l^T \Pi^T \tilde{v} + \tilde{v}^T \Pi a \Pi^T \tilde{v} \\ &= \|l\|_a^2 + v^T \tilde{v} = \|l\|_a^2 + \|v\|_{\tilde{a}}^2 \leq \|v\|_{\tilde{a}}^2. \end{aligned}$$

So the conclusion holds and the optimal solution is $u^* = a \Pi^T \tilde{v}$. \square

The following theorem is a direct consequence of the above result.

THEOREM 2. *The Lagrangian (3.19) is equivalent to*

$$(3.21) \quad L(x, y) = \frac{1}{2} \|y - \tilde{b}(x)\|_{\tilde{a}}^2.$$

So, the Lagrangian (3.19) and the action functional are independent of the embedding in the ambient space.

Following section 2, we have that the corresponding Hamiltonian for (3.19) is

$$(3.22) \quad H(x, p) = \langle \Pi b(x), p \rangle + \frac{1}{2} \|\sigma(x)^T \Pi^T p\|^2,$$

where $\langle \cdot, \cdot \rangle$ and $\|\cdot\|$ are the inner product and 2-norm of \mathbb{R}^n , respectively. To verify that (3.22) is the Legendre transformed L , we use the duality theory of optimization and shall show that for any fixed $x \in \mathcal{M}$ and $y \in T_x \mathcal{M}$,

$$(3.23) \quad \begin{aligned} L(x, y) &= \sup_{p \in \mathbb{R}^n} \left(\langle y, p \rangle - H(x, p) \right) \\ &= \sup_{p \in \mathbb{R}^n} \left(\langle y - \Pi b(x), p \rangle - \frac{1}{2} \|\sigma(x)^T \Pi^T p\|^2 \right). \end{aligned}$$

The Lagrange function $\mathcal{L} : \mathbb{R}^n \times \mathbb{R}^n \rightarrow \mathbb{R}$ associated with the constrained optimization problem for the variable u in (3.19) is as follows:

$$\mathcal{L}(u, \lambda) = \frac{1}{2} \|u\|_a^2 - \langle \lambda, \Pi u - y + \Pi b(x) \rangle,$$

where $\lambda \in \mathbb{R}^n$ is the Lagrange multiplier. The dual function $g(\lambda) = \min_{u \in \mathbb{R}^n} \mathcal{L}(u, \lambda)$. Straightforward calculation for this minimization shows $g(\lambda) = \mathcal{L}(a \Pi^T \lambda, \lambda) = -\frac{1}{2} \|\sigma^T \Pi^T \lambda\|^2 + \langle \lambda, y - \Pi b(x) \rangle$. Since the strong duality holds for the quadratic programming in (3.19), we have that $L(x, y) = \sup_{\lambda \in \mathbb{R}^n} g(\lambda)$, which is exactly (3.23) by identifying p as λ . It is not difficult to show that for finite $L(x, y)$, the optimal p^* in (3.23) is in $\text{Img}(\Pi)$. So, the Hamiltonian $H(x, p)$ in (3.22) is finite for $x \in \mathcal{M}$ and $p \in T_x \mathcal{M}$ and is equal to $-\infty$ otherwise.

By the duality theory, we also have that

$$(3.24) \quad \frac{\partial L}{\partial y} = p^* \quad \text{and} \quad u^* = a \Pi^T p^*,$$

where u^* is the minimizer of (3.19). It is also observed that p^* is the unique solution (in $\text{Img}(\Pi)$) of $\tilde{a} p^* = y - \Pi b(x)$ since $\Pi a \Pi^T p^* = \Pi u$.

3.4. Geometric action functional on \mathcal{M} . The geometric formulation of the action function, developed in [10], does not involve time explicitly but allows the variation of the time interval. If we consider the original formulation of Freidlin–Wentzell theory as an analogy of Lagrangian mechanics for the trajectory of a particle, then the geometric action functional in [10] corresponds to the Maupertuis principle (section 44 in [14]) for the curve along which the particle travels.

In the following, we consider the geometric action functional \hat{S} for the SDE (3.13) on the manifold \mathcal{M} . Suppose that a curve γ on \mathcal{M} is parametrized as $\gamma = \varphi(\alpha)$, with $\alpha \in [0, 1]$, for instance, α being the normalized arc-length parameter. Then the geometric action functional is the line integration along γ

$$\hat{S}[\varphi] = \int_{\gamma} \langle p, d\varphi \rangle$$

subject to the constraint $H(\varphi, p) = 0$, where $p = \partial L / \partial y(\varphi, \dot{\varphi})$ is the generalized momentum, L is the Lagrangian defined in (3.23), and $\dot{\varphi}$ is the time derivative. By (3.24), this generalized momentum satisfies $\tilde{a}p = y - \Pi b(x)$, and

$$(3.25) \quad p = \tilde{a}^{-1}(\dot{\varphi} - \Pi b(\varphi)).$$

So, \hat{S} has the following expression:

$$\begin{aligned} \hat{S}[\varphi] &= \int \langle \tilde{a}^{-1}(\dot{\varphi} - \Pi b(\varphi)), d\varphi \rangle \\ &= \int_0^1 \langle \tilde{a}^{-1}(\varphi' \lambda - \Pi b(\varphi)), \varphi' \rangle d\alpha, \end{aligned}$$

where the scalar-valued function $\lambda := d\alpha / dt \in [0, +\infty]$ is the change of variable between the physical time t and the arc length α . Here $\dot{\varphi} = d\varphi / dt$ is the time derivative and $\varphi' = d\varphi(\alpha) / d\alpha$ is the tangent vector of the curve for the α -parametrization. To derive the expression of λ in terms of φ and φ' , we use the condition that the Hamiltonian along the path is constant zero [10, 14] as well as the formula for p in (3.25):

$$H(\varphi, p) = \frac{1}{2} \langle \dot{\varphi} + \Pi b(\varphi), \dot{\varphi} - \Pi b(\varphi) \rangle_{\tilde{a}} = \frac{1}{2} \|\dot{\varphi}\|_{\tilde{a}}^2 - \frac{1}{2} \|\Pi b(\varphi)\|_{\tilde{a}}^2 = 0.$$

Since $\dot{\varphi} = \varphi' \lambda$, the above equation gives the important quantity

$$(3.26) \quad \frac{d\alpha}{dt} = \lambda = \frac{\|\tilde{b}\|_{\tilde{a}}}{\|\varphi'\|_{\tilde{a}}}.$$

Therefore, we obtain the expression of \hat{S} for $\varphi \in \mathcal{A}$,

$$\begin{aligned} \hat{S}[\varphi] &= \int_0^1 \left\langle \tilde{a}^{-1} \left(\varphi' \frac{\|\tilde{b}\|_{\tilde{a}}}{\|\varphi'\|_{\tilde{a}}} - \Pi b(\varphi) \right), \varphi' \right\rangle d\alpha \\ (3.27) \quad &= \int_0^1 \|\tilde{b}(\varphi)\|_{\tilde{a}} \|\varphi'\|_{\tilde{a}} - \langle \tilde{b}(\varphi), \varphi' \rangle_{\tilde{a}} d\alpha. \end{aligned}$$

This expression can also be obtained from the time-parametrized $S_T^{\mathcal{M}}$ in (C.3) by using (3.26). Proposition 4 allows us to write (3.27) equivalently in the following a -norm:

$$(3.28) \quad \hat{S}[\varphi] = \int_0^1 \|\Pi^{-1} \tilde{b}(\varphi)\|_a \|\Pi^{-1} \varphi'\|_a - \langle \Pi^{-1} \tilde{b}(\varphi), \varphi' \rangle_a d\alpha.$$

We recall that $\Pi^{-1} \tilde{b} = \Pi^{-1} \Pi b$ is not equal to b .

The Euler–Lagrange equation for the geometric action functional \hat{S} can be obtained directly from the variational calculus or by using (3.26) to transform the Euler–Lagrange equation for $S_T^{\mathcal{M}}$ into arc-length parametrized form. For the same curve $\gamma = \{\phi(t) : t \in [0, T]\} = \{\varphi(\alpha) : \alpha \in [0, 1]\}$, where $d\alpha/dt = \lambda$ is given by (3.26), the following general result holds for the Fréchet derivative of two functionals $S^{\mathcal{M}}$ and \hat{S} :

$$\frac{\delta \hat{S}}{\delta \varphi} = \lambda^{-1} \frac{\delta S_T^{\mathcal{M}}}{\delta \phi}.$$

Thus, by (C.9) and (3.26)

$$(3.29) \quad \frac{\delta \hat{S}}{\delta \varphi} = \lambda^{-1} \left(-\tilde{p}'\lambda - \tilde{J}^T \tilde{p} + \frac{1}{2}(\tilde{a}\tilde{p}) \otimes (\tilde{a}\tilde{p}) : \nabla(\tilde{a}^{-1}) \right),$$

where $\tilde{p} = \tilde{a}^{-1}(\phi'\lambda - \tilde{b})$.

We finish this section by presenting a spherical manifold case which will be used later.

Example 1 (sphere \mathbb{S}^d). Using the result in Example 3, we have the form of the action functional $S_T^{\mathcal{M}}$ in (C.2):

$$S_T^{\mathcal{M}}[\phi] = \frac{1}{2} \int_0^T \left\| \dot{\phi} - \Pi b(\phi) \right\|_a^2 - \left\langle \frac{\phi}{\|\phi\|_a}, \dot{\phi} - \Pi b(\phi) \right\rangle_a^2 dt.$$

Note that the first term is exactly S_T^1 of (C.5), so $S_T^{\mathcal{M}}[\phi] \leq S_T^1[\phi]$. Likewise, we have the expression of the geometric action function (3.28) in this case, which is

$$\begin{aligned} \hat{S}[\varphi] = \int_0^1 & \sqrt{\left(\|\Pi b\|_a^2 - \langle \Pi b, \varphi \rangle_a^2 / \|\varphi\|_a^2 \right) \left(\|\varphi'\|_a^2 - \langle \varphi', \varphi \rangle_a^2 / \|\varphi\|_a^2 \right)} \\ & - \langle \Pi b, \varphi' \rangle_a + \langle \Pi b, \varphi \rangle_a \langle \varphi', \varphi \rangle_a / \|\varphi\|_a^2 d\alpha. \end{aligned}$$

4. Constrained minimum action method. The least action principle is to solve the constrained minimization problem, (C.2),

$$\inf_{\phi \in \mathcal{A}} S_T^{\mathcal{M}}[\phi] = \inf_{\phi \in \mathcal{A}} \frac{1}{2} \int_0^T \left\| \Pi^{-1}(\dot{\phi} - \Pi b) \right\|_a^2 dt$$

and the geometric version, (3.28),

$$\inf_{\phi \in \mathcal{A}} \hat{S}[\varphi] = \inf_{\phi \in \mathcal{A}} \int_0^1 \left\| \Pi^{-1} \Pi b \right\|_a \|\Pi^{-1} \varphi'\|_a - \langle \Pi^{-1} \Pi b, \varphi' \rangle_a d\alpha.$$

The Euler–Lagrange equations have been derived in section 3. Thus, in principle, the minimum action paths can be calculated by any numerical optimization solver, such as the steepest descent dynamics. In the following, we briefly discuss many practical aspects of this computational problem. Many of them have already been investigated in the context without constraints during the development of the minimum action method [8, 25, 10, 23, 22, 21]. Some of these techniques are quite important for large-scale problems. The consideration of the constraints in the constrained minimum action method will also be discussed in detail.

First recall that one of our motivations for the manifold case is for the constraints specified by the nondegenerate constraint functions $c_k(x) = 0$, $k = 1, 2, \dots, n - d$,

as discussed in Proposition 1. Thus the manifold $\mathcal{M} = \{x \in \mathbb{R}^n : c_k(x) = 0, k = 1, 2, \dots, n-d\}$ and the projection Π is the orthogonal projection $P = I - G^T(GG^T)^{-1}G$ in (3.9). The inverse of \tilde{a} appearing in the Euler–Lagrange equation can be calculated via $a^{-1}\Pi^{-1}$ as shown in Proposition 3. The explicit formula for Π^{-1} is usually solved from its definition. The basis vector for the space $\text{Ker}(\Pi_x)$ is $\xi_k = \nabla c_k(x)$. The explicit formula of Π^{-1} under a -norm can be expressed in terms of $\xi_k = \nabla c_k$, following the same procedure as in Proposition 7. We also mention that when the local coordinate representations for \tilde{a}^{-1} are conveniently available for some special problems, the corresponding local coordinate form for the action functional (C.2) and (3.28) can be derived and used to have a standard nonlinear optimization problem without constraints.

The first thing to consider in any numerical scheme for the action functionals (C.2) and (3.28) and their Euler–Lagrange equations (C.9) and (3.28), respectively, is the “spatial” discretization for t or α . For Freidlin–Wentzell action functional (C.2), the path to compute is represented as $\phi = (\phi_0, \phi_1, \phi_2, \dots, \phi_N)$ for a given time mesh grid $0 = t_0 < t_1 < t_2 \dots < t_N = T$ such that $\phi_i \approx \phi(t_i)$. It is important to maintain a good parametrization for the path in the configuration space to ensure good accuracy; thus, the idea of the adaptive minimum action method (aMAM) in [25] should also be applied here. The aMAM uses the moving mesh method to redistribute the time mesh grid $\{t_i\}$ when the current mesh grid does not meet certain criteria, for instance, when the ratio $\max_i \|\phi_{i+1} - \phi_i\| / \min_i \|\phi_{i+1} - \phi_i\|$ exceeds some threshold ($1.5 \sim 5$ in practice). The aMAM solves a one-dimensional elliptic equation to obtain the numerical mapping between the time $t \in [0, T]$ and a new variable $\alpha \in [0, 1]$ (a similar role for the arc-length parameter in some sense, but more flexible). The key element in this moving mesh strategy is the monitor function w , which is typically chosen as $\|\dot{\phi}\|$ to achieve arc-length parametrization for the discrete path. The alternative choice with a similar effect is to choose $w(t) = \|b(\phi)\|_{\tilde{a}}$ by noting that the minimum path satisfies $\|\dot{\phi}\|_{\tilde{a}} = \|\tilde{b}\|_{\tilde{a}}$ for the zero-valued Hamiltonian. The flexibility of selecting other types of the monitor function w caters for other needs, for example, including the second derivative $\|\partial_\alpha^2 \phi\|^{-1}$ in w to place more points in regions of high curvature.

Besides the redistribution of the mesh grid, the first and second derivatives of the path can be calculated by the finite difference method as aMAM [25] did or by the more advanced spectral element method proposed in [22] to achieve higher accuracy.

For the gMAM to solve (3.28), the curve γ is represented by $(\varphi_0, \varphi_1, \dots, \varphi_N)$, and the above “spatial” discretization methods are all applicable in this geometric setting. Likewise, the progress of the path evolution will eventually deteriorate the mesh quality. Thus it is equally important as in aMAM to check the ratio $\max_i \|\varphi_{i+1} - \varphi_i\| / \min_i \|\varphi_{i+1} - \varphi_i\|$ and perform reparametrization by interpolation when necessary.

For the calculation of the arc length of the curve $\varphi(\alpha)$, it may be more natural to use the geodesic distance on \mathcal{M} to define the arc length, but it is practically convenient to just use the Euclidean arc length. If the number of discrete images in representing the curve is sufficiently large, these two choices of the distance between neighboring images measured by geodesic or Euclidean metrics would not give much difference.

After the temporal mesh or arc-length mesh is redistributed, the interpolation can be implemented by the cubic spline interpolation like in [8, 25]. Since for the non-gradient system, the path usually has a sharp corner on the basin boundary, the high curvature there would decrease the interpolation accuracy. The well-known WENO interpolation is quite a feasible and efficient method to handle the discontinuous second derivative (w.r.t arc length α or the α variable in aMAM).

In the end, we discuss the issue of how to take care of the constraints. We select a numerical scheme for the constrained nonlinear optimization, say, the augmented Lagrangian method [18], which requires the input of an objective function, constraint functions, and their gradients. In our constrained minimum action method, the objective function is the discretized version of the action functional $S[\phi_0, \phi_1, \dots, \phi_N]$, where $\phi_0 = A$, $\phi_N = B$ are given on \mathcal{M} . The derivative of the objective function is calculated by the Fréchet derivative of the action functional, i.e., the Euler–Lagrange equation (unconstrained version on \mathbb{R}^n). The constraints are $c_k(\phi_i) = 0 \quad \forall k = 1, \dots, n-d$ and $i = 1, \dots, N-1$, totally $(n-d)(N-1)$ constraints. Their gradients can usually be derived analytically for specific problems; otherwise, the derivative-free optimization solvers have to be used. The augmented Lagrangian method solves the constrained problem by sequentially solving unconstrained problems

$$\min_{\phi} \left(S[\phi] - \sum_{k,i} \lambda_{ki} c_k(\phi_i) + \frac{\mu}{2} \sum_{k,i} c_k^2(\phi_i) \right)$$

and updating the Lagrange multipliers λ_{ki} and the penalty factor μ . When the path is parametrized in time, the above S is $S_T^{\mathcal{M}}$. During solving this constrained optimization problem for a given mesh grid in $[0, T]$, the mesh quality will be checked, and when the adjustment for the mesh is needed, the mesh will be redistributed and the path after interpolation will be used as the initial guess for the constrained discrete optimization problem associated with the updated time mesh grid. When using the geometric action functional \hat{S} , the arc-length distribution of the discrete images on the curve can be achieved in an alternative approach, rather than using interpolation in the above aMAM idea; we furthermore impose $N-1$ constraints for the arc-length parametrization requirement: $\|\varphi_{i+1} - \varphi_i\|^2 = \|\varphi_i - \varphi_{i-1}\|^2$ for $i = 1, \dots, N-1$. In this way, the initial curve does not have to be exactly on the manifold or even arc-length parametrized to satisfy all the constraints. The augmented Lagrangian method will take care of both types of constraints. The calculations in the next section for our examples of interest in this paper are implemented by calling the MATLAB `fmincon` subroutine and incorporating the above two types of constraints.

One can also use the projected steepest descent dynamics to solve the constrained optimization problem, that is, to solve the Euler–Lagrange equation, i.e.,

$$\partial_{\tau} \phi(\tau, t) = -\Pi \frac{\delta S}{\delta \phi}.$$

This requires that the initial guess of the path $\phi(0, \cdot)$ should satisfy the constraints $\{c_k = 0\}$. The projection Π is explicitly placed on the right-hand side to suppress the “spatial” discretization error amounting to small deviation from the tangent space. However, the τ -discretization will also bring a small deviation from the manifold, even when the force at τ_n is exactly on the tangent space. Thus, it is favored to bring $\tilde{\phi}^{(n+1)} = \phi^{(n)} - \delta\tau \cdot (\Pi \frac{\delta S}{\delta \phi})^{(n)}$ back to the manifold exactly so that the obtained $\phi^{(n+1)}$ is on \mathcal{M} . This cannot be done via the projection Π on tangent space and indeed it may be quite challenging for certain problems. But sometimes, for the examples in our following section where the manifold is typically a sphere \mathbb{S}^d , this procedure is quite easy and a simple normalization $x \rightarrow x/\|x\|$ works well. For general situations, [6] offered a proposal of using the implicit scheme for τ in developing the constrained string method. A similar idea is to introduce components in normal space, $\text{span}\{\nabla c_k\}$, to correct the error from $\delta\tau$: to look for $\gamma_1, \dots, \gamma_{n-d}$ such that

$c_k(\phi^{(n+1)}) = c_k(\tilde{\phi}^{(n+1)} + \gamma_j \nabla c_j(\phi^{(n)})) = 0 \forall k$. Overall, both of these methods eventually bring some overhead of solving nonlinear equations for $\phi^{(n+1)}$.

The last comment is about the choice of the initial path. Like any optimization problem, the choice of a good initial path is essential to find the *global* minimizer and this is the biggest difficulty for many practical problems with multiple local minimizers. The general strategy we used for path-finding problems is to explore the configuration space by using the minimum action method with simple guesses such as straight lines. With a more clear understanding about the invariant structures such as saddle points, heteroclinic orbits, etc., some new initial guesses can be proposed to try in hope of new information about the configuration space. These two tasks actually benefit each other. Usually, by this recursive procedure, one can both gain deep insights of the configuration space and obtain the path whose action is as small as possible. The details for specific examples can be found in the next section or the previous work [23].

5. Examples. In this section, we apply the constrained minimum action method to study the transition pathways for the motion of one class of liquid crystal molecules. These types of macromolecules are usually modeled as rigid rods so the configuration space for each rod is \mathbb{S}^2 . More realistic models such as general bead-rod-spring models have more complex intrinsic constraints for the molecular configurations; the details are well-explained in Chapter 5 of [19]. The rigid rod model we are studying here is the typical building block for those chain models.

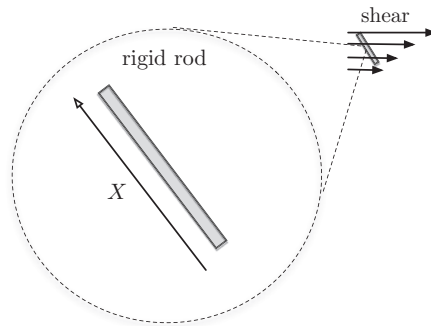


FIG. 1. *Rigid rod polymeric model in shear flow. The length of the directed vector \mathbf{X} is one.*

Typically, there are many equilibrium states for the molecular configurations. Depending on the interaction between molecules, there could be some spontaneously preferred directions \mathbf{X} for the molecules. In many cases where the ensemble statistics are of interest, the direction \mathbf{X} and $-\mathbf{X}$ is undistinguished due to symmetry. But at a microscopical level, each individual configuration does switch between the symmetric two metastable states \mathbf{X} and $-\mathbf{X}$. When these macromolecular polymers are added into solvent (Figure 1), then the mixed solution has interesting hydrodynamic and rheological features different from the Newtonian fluid. The study of complex fluid mainly focuses on macroscopic quantities of polymeric fluid, such as viscoelasticity. However, the change of macromolecular configurations at the microscopic level due to thermal fluctuation and fluid shear is of its own interest, in particular when these macromolecules, for instance, liquid crystals, are directly responsible for some physical mechanisms in practice, such as color control for display devices.

In the following, we present two examples to understand the transition paths

in the rigid rod model. In the first example, we study the single rod molecule with quadratic potential in shear flow. Due to spherical symmetry, any linearly stable state \mathbf{X} has a symmetric stable one $-\mathbf{X}$. The transition from \mathbf{X} to $-\mathbf{X}$ corresponds to the flip over process of the rod molecule. How the shear rate impacts this flip over process is our interest. Our second example includes two rods with interaction between them. This is the simplest case for the weakly interaction particle system [16]. To see how the anisotropic diffusion tensor play roles transition path, we artificially assign two different diffusion coefficients, σ_1 and σ_2 , for the two rods and investigate the effect of the ratio σ_2/σ_1 on the transition pathways. Although the diffusion coefficient (i.e., temperature) of two molecules seem to be the same in physical reality, our manipulation of anisotropic noise in this model produces some interesting results, which could be instructive in the general case of the state-dependent noise $\sigma(x)$ and may be quite useful when the precise control of noise size for each individual rod (or two groups of rods) is possible.

Last, we remark that we only report the results from the constrained minimum action method based on the geometric action formulation. Thus, the objects we calculated are curves in the phase space. The pathways from the constrained Freidlin–Wentzell action functional are consistent with these results when the underlying time interval is sufficiently large.

5.1. Flip over process of one rigid rod. Consider a unit sphere \mathbb{S}^2 in \mathbb{R}^3 . $X = (X_1, X_2, X_3) \in \mathbb{R}^3$. Let $V : \mathbb{R}^3 \rightarrow \mathbb{R}$ be the potential energy with symmetry $V(x) = V(-x)$ and W_t be a Brownian motion in \mathbb{R}^3 . Write the normal vector $\mathbf{n}(x) = x/\|x\| \in \mathbb{S}^2$. The motion of the rod molecule in consideration is described by the equation

$$dX = (I - \mathbf{n}(X)\mathbf{n}(X)^\top) \left((-\nabla V(X) + K_0 X) dt + \sqrt{\varepsilon} \circ dW_t \right),$$

where K_0 is the matrix of the shear rate tensor in the Cartesian coordinate.

Here the noise is isotropic and the manifold \mathcal{M} is \mathbb{S}^2 . The geometric action functional in (3.28) is reduced to

$$\begin{aligned} \hat{S}[\varphi] &= \int_0^1 \|\Pi^{-1}\Pi b(\varphi)\| \|\Pi^{-1}\varphi'\| - \langle \Pi^{-1}\Pi b(\varphi), \varphi' \rangle d\alpha \\ (5.1) \quad &= \int_0^1 \|\Pi b(\varphi)\| \|\varphi'\| - \langle \Pi b(\varphi), \varphi' \rangle d\alpha, \end{aligned}$$

where $\|\varphi(\alpha)\| = 1 \forall \alpha$.

We assume the following quadratic form of the external potential function V :

$$(5.2) \quad V(x) = \sum_{i=1}^3 \frac{1}{2} \mu_i x_i^2, \text{ where } \mu_3 > \mu_2 > \mu_1 > 0.$$

The two local minima of V on \mathbb{S}^2 are $e^{(1)} = (1, 0, 0)$ and $-e^{(1)} = (-1, 0, 0)$; the two local maxima are $e^{(3)} = (0, 0, 1)$ and $-e^{(3)} = (0, 0, -1)$; the saddles are $e^{(2)} = (0, 1, 0)$ and $-e^{(2)} = (0, -1, 0)$. In the example below, we simply set $(\mu_1, \mu_2, \mu_3) = (1, 2, 3)$.

For the quadratic potential equation (5.2), the SDE then becomes the following form:

$$(5.3) \quad dX = (I - \mathbf{n}(X)\mathbf{n}(X)^\top)(KX dt + \sqrt{\varepsilon} \circ dW_t),$$

where $K = \text{diag}\{\mu_1, \mu_2, \mu_3\} + K_0$. We consider two forms of shear rate matrix K_0 corresponding to different directions of the shear flow.

5.1.1. Shear flow: Example 1. We first consider the following shear flow, where x_1 is the streamwise direction, x_2 is the shearwise direction, and x_3 is the spanwise direction. So it is assumed that

$$(5.4) \quad K_0 = \begin{bmatrix} 0 & \dot{\gamma}_{12} & 0 \\ 0 & 0 & 0 \\ 0 & 0 & 0 \end{bmatrix}.$$

Here the shear rate $\dot{\gamma}_{12}$ is a constant parameter.

The deterministic drift flow on \mathbb{S}^2 is $\dot{X} = (I - \mathbf{n}\mathbf{n}^\top)KX$. The fixed points of this flow are the three vectors on \mathbb{S}^2 ,

$$(5.5) \quad \begin{aligned} \mathbf{n}^{(1)} &= (1, 0, 0)^\top, \\ \mathbf{n}^{(2)} &= (-\dot{\gamma}_{12}, \mu_2 - \mu_1, 0)^\top / \sqrt{\dot{\gamma}_{12}^2 + (\mu_2 - \mu_1)^2}, \\ \mathbf{n}^{(3)} &= (0, 0, 1)^\top, \end{aligned}$$

and their symmetric counterparts $-\mathbf{n}^{(i)}$, $i = 1, 2, 3$. In total, there are three pairs of fixed points. Since $\mu_3 > \mu_2 > \mu_1 > 0$ in the quadratic potential, (5.2), we can derive the following linear stability results for infinitesimal perturbations. The pair $\pm\mathbf{n}^{(1)}$ is linearly stable (classified as *sink* and denoted as si_+ and si_- , respectively) with two stable eigen directions $\mathbf{e}^{(2)}$ and $\mathbf{e}^{(3)}$. The pair of $\pm\mathbf{n}^{(3)}$ is linearly unstable (classified as *source* and denoted as so_+ and so_- , respectively). The pair of $\pm\mathbf{n}^{(2)}$ is saddle point (denoted as sa_+ and sa_- , respectively) with one stable eigen direction $\mathbf{e}^{(3)}$ (the unstable eigen direction relies on $\dot{\gamma}_{12}$). The separatrix on the unit sphere between the two sources si_+ and si_- is the great circle of \mathbb{S}^2 in the plane spanned by sa_\pm and so_\pm .

The introduction of the shear rate in form of (5.4) only affects the orientation of the saddle point, (5.5). The positive value of shear rate $\dot{\gamma}_{12}$ has the effect of rotating the saddle direction $\mathbf{n}^{(2)}$ counterclockwise (looking down from the x_3 -direction, i.e., vertical direction). The negative $\dot{\gamma}_{12}$ gives the opposite rotation direction.

We are concerned with the flip over process of the rigid rod, i.e., the transition between two symmetric stable fixed points $si_+ = \mathbf{n}^{(1)}$ and $si_- = -\mathbf{n}^{(1)}$. The minimal action for this transition is related to the frequency of this process ($\propto \exp(-\inf S/\varepsilon)$ [9]). The smaller the minimal action, the more frequently the rod flips between two stable states.

To resolve all possible minimizers of the variational problem $\inf_{\varphi \in \mathbb{S}^2} \hat{S}[\varphi]$, the initial guesses of the path should be carefully constructed. The idea of setting the initial guess is as follows. Since on the separatrix between si_+ and si_- there are four fixed points, so_\pm and sa_\pm , we then construct the different initial paths passing through these points, respectively. In consideration of the symmetry for the case of so_\pm , we only need to test three different initial guesses, which give three different local minima of the action functional \hat{S} . As a result, the obtained three minima correspond to the minimal actions from si_+ to saddles sa_- , sa_+ , and so_- (or so_+), respectively. The minimum among these three minimized actions gives the global optimum and thus corresponds to the correct transition path between si_- and si_+ . Refer to Figure 2 for the plot of these three actions when the shear rate is varied. This evidence shows that the shear of the flow field lowers the global minimum of the action and hence increases the flip over frequency. At a high shear rate, the frequency could be so large that the rod molecule would oscillate between the directions $si_- = -\mathbf{n}^{(1)}$ and $si_+ = \mathbf{n}^{(1)}$.

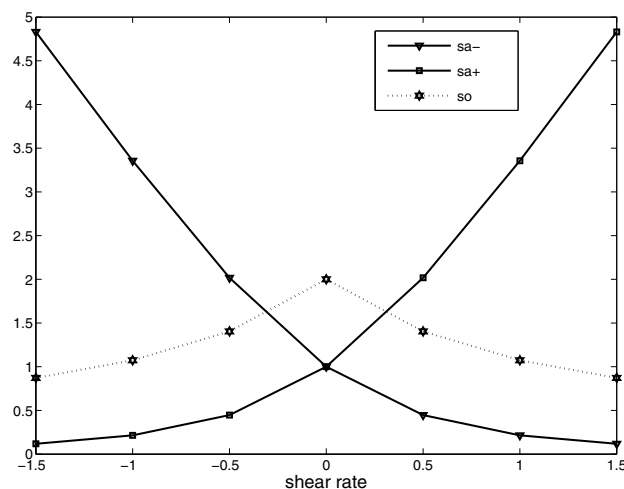


FIG. 2. The minimum actions (vertical axis) for three paths from si_+ to sa_- , sa_+ and so_{\pm} , respectively.

Among the obtained three paths from different initial guesses, the global minimum is the one passing the saddle sa_- or sa_+ , depending on the direction of the shear, i.e., the sign of $\dot{\gamma}_{12}$. These paths are one of semi great circles entirely in the x_1 - x_2 plane. Figure 3 shows the global minimum action path starting from si_+ for $\dot{\gamma}_{12} = 0, 1, -1$. For instance, when $\dot{\gamma}_{12} > 0$, the saddle sa_- (the solid black line) is shifted closer to si_+ so that it takes less action for the system to escape from si_- to the separatrix by selecting this saddle sa_- . A similar picture holds for negative $\dot{\gamma}_{12}$, where the saddle sa_+ (the dashed black line) is shifted closer to si_+ .

5.1.2. Shear flow: Example 2. Next we study the transitions with the following shear rate tensor:

$$K_0 = \begin{bmatrix} 0 & 0 & \dot{\gamma}_{13} \\ 0 & 0 & 0 \\ 0 & 0 & 0 \end{bmatrix}.$$

The fixed points for this K_0 become

$$\begin{aligned} \mathbf{n}^{(1)} &= (1, 0, 0)^T, \\ \mathbf{n}^{(2)} &= (0, 1, 0)^T, \\ \mathbf{n}^{(3)} &= (-\dot{\gamma}_{13}, 0, \mu_3 - \mu_1)^T / \sqrt{\dot{\gamma}_{13}^2 + (\mu_3 - \mu_1)^2}, \end{aligned}$$

and $si_- = -\mathbf{n}^{(1)}$ and $si_+ = \mathbf{n}^{(1)}$ are sinks, $sa_- = -\mathbf{n}^{(2)}$ and $sa_+ = \mathbf{n}^{(2)}$ are saddles, $so_- = -\mathbf{n}^{(3)}$ and $so_+ = \mathbf{n}^{(3)}$ are sources. The heteroclinic orbits among these fixed points are similar to the previous example in section 5.1.1: They are the great circles connecting the neighboring fixed points. The separatrix between si_+ and si_- is also the great circle in the plane of sa and so . The difference from the example in section 5.1.1 is that now the shear rate affects the location of the sources so_{\pm} , while the saddles sa_{\pm} are unchanged.

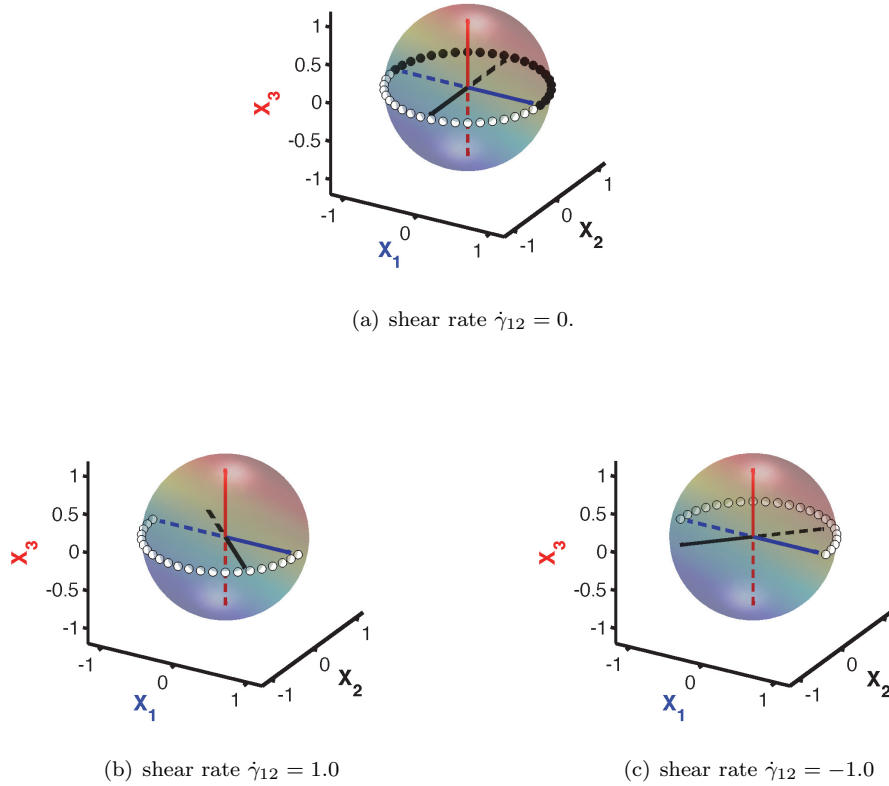


FIG. 3. Global minimum action paths for different shear rates. The two symmetric flip over paths passing sa_- are shown in white and black, respectively.

Again, we are interested in the transition from si_+ to si_- and shall examine the minimum action paths with different initial guesses which pass through the fixed points so_- , so_+ , and sa_{\pm} , respectively. Figure 4 shows the minimum actions for these three paths. From this figure, we can observe that a larger shear rate decreases the actions both to the saddle and to the source. However, there is a competition between these two local minima of the action. When the shear rate is small, the path passing the saddle is the global solution. But when the shear rate is very large, the calculation shows that the action to the source can be slightly smaller than the one to the saddle so that the transition state changes from the saddle to the source. This suggests that there is a bifurcation point of the parameter $\dot{\gamma}_{13}^*$ (around 1.9 for this example in our calculation) for the patterns of the global minimum action path.

The above conclusion can be better understood if we plot the global minimum action path for $\dot{\gamma}_{13} = 1$ and 2 in Figure 5. The positive value of shear rate $\dot{\gamma}_{13}$ has the effect of tilting the unstable fixed point $so_+ = \mathbf{n}^{(3)}$ (the solid red line) counterclockwise in the x_1 - x_3 plane (looking from the $-x_2$ -direction). Such tilts will pull so_- (the dashed red line) toward si_+ (the solid blue line) and push so_+ away from si_+ . However, when the shear rate is not strong, this push is not significant enough to

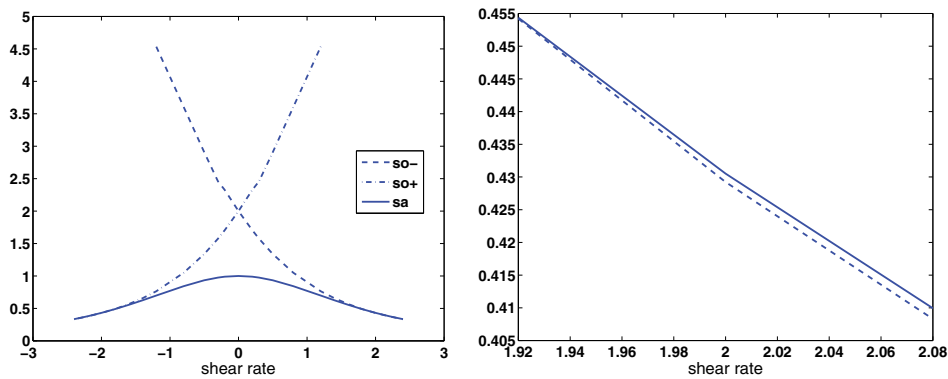


FIG. 4. The minimum actions for three paths from si_+ to so_- , so_+ , and sa_{\pm} (either sa_- or sa_+ since the minimal actions are the same due to symmetry), respectively. When $\dot{\gamma}_{13}$ passes the critical value $\dot{\gamma}_{13}^* \approx 1.9$, the global minimum path changes from passing sa to passing so_- , i.e., the transition state changes from sa to so_- . The right panel is the zoom of the left panel for a window near $\dot{\gamma}_{13} = 2$.

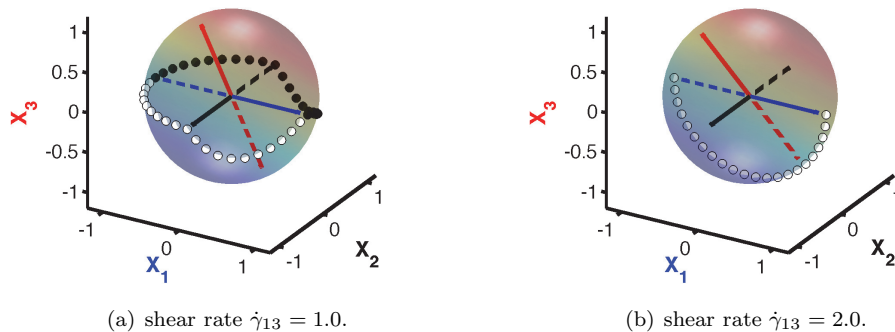


FIG. 5. Global minimum action paths for different shear rates. (a) The transition path from si_+ to si_- through sa_+ and its symmetric mirror are both shown. (b) The path is the semicircle in the plan spanned by so and si (x_1 - x_3 plane). The initial guess of the path in the minimum action method is the path in (a).

beat the action of the path through the saddle sa_{\pm} (the pair of curves shown in Figure 5(a)). When $\dot{\gamma}_{13}$ continues to increase by passing the critical value $\dot{\gamma}_{13}^*$, the shear-induced tilt will become strong enough to lower the action to reach so_- significantly so as to become a global solution.

In summary, when the shear of the fluid affects the unstable fixed points so_{\pm} of the molecular configuration on S^2 , the competition of the minimum action paths passing through the saddle sa_{\pm} or through the source so_{\pm} would generate a bifurcation of the patterns of the global path. The same phenomena have been observed before, for instance, in some planer (nongradient) system [17]. For real problems, the shear rate tensor K_0 may be the combination of the above two examples we have studied; from the analysis above, we expect that the similar bifurcation of the pathways could happen for a different size of the shear rate. It is also generally believed that the shear

would lower the global minimum action and thus increase the flip over frequency.

5.2. Flip over of two rigid rods. Here, we study a slight generalization of the previously studied single rod case, a toy model of two interactive rigid rods. Let $\mathbf{X}_1, \mathbf{X}_2$ be the directed unit vector of two rods. We consider the following stochastic dynamics on $\mathbb{S}^2 \times \mathbb{S}^2$:

$$(5.6) \quad \begin{cases} d\mathbf{X}_1 = (I - \mathbf{n}_1 \mathbf{n}_1^T)(-\nabla V(\mathbf{X}_1) dt - \nabla_{\mathbf{x}_1} U(\mathbf{X}_1, \mathbf{X}_2) dt + \sigma_1 \sqrt{\epsilon} \circ d\mathbf{W}_1), \\ d\mathbf{X}_2 = (I - \mathbf{n}_2 \mathbf{n}_2^T)(-\nabla V(\mathbf{X}_2) dt - \nabla_{\mathbf{x}_2} U(\mathbf{X}_1, \mathbf{X}_2) dt + \sigma_2 \sqrt{\epsilon} \circ d\mathbf{W}_2), \end{cases}$$

where $\mathbf{n}_i = \mathbf{X}_i / \|\mathbf{X}_i\|$, $i = 1, 2$; σ_1 and σ_2 are two positive constants. Here $U(\mathbf{x}_1, \mathbf{x}_2) : \mathbb{S}^2 \times \mathbb{S}^2 \rightarrow \mathbb{R}$ describes the interactions of these two rods. One common choice of this potential U is the Maier-Saupe potential

$$(5.7) \quad U(\mathbf{x}_1, \mathbf{x}_2) = A \sin^2(\theta - \theta_0),$$

where θ is the angle between \mathbf{x}_1 and \mathbf{x}_2 (Figure 6), A is a positive number, and θ_0 is the preferred angle. We assume $\theta_0 = 0$ without loss of generality.

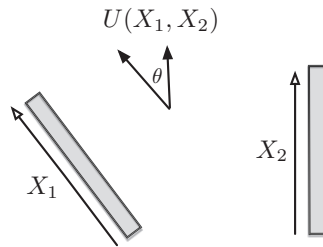


FIG. 6. Two rigid rods with interaction potential U .

The model we are studying in (5.6) has no effect of shear flow and is a reversible system when $\sigma_1 = \sigma_2$. In the following, we are interested in how different values of the ratio σ_2/σ_1 affect the transition paths. First we give the action functional form for this example. We write the path as a pair $\varphi = [\varphi_1, \varphi_2] \in \mathbb{R}^3 \times \mathbb{R}^3$. Denote $b(\varphi) = [b_1(\varphi), b_2(\varphi)] \in \mathbb{R}^3 \times \mathbb{R}^3$, where $b_i(\varphi) = -\nabla V(\varphi_i) - \nabla_{\mathbf{x}_i} U(\varphi_1, \varphi_2)$ corresponds to the rod i . The geometric action functional (3.28) for (5.6) thus has the following form:

$$(5.8) \quad \hat{S}[\varphi] = \int_0^1 \sqrt{\frac{\|b_1\|^2}{\sigma_1^2} + \frac{\|b_2\|^2}{\sigma_2^2}} \sqrt{\frac{\varphi_1'^2}{\sigma_1^2} + \frac{\varphi_2'^2}{\sigma_2^2}} - \frac{\langle b_1, \varphi_1' \rangle}{\sigma_1^2} - \frac{\langle b_2, \varphi_2' \rangle}{\sigma_2^2} d\alpha.$$

The constraint is $\|\varphi_1\| = \|\varphi_2\| = 1$.

We choose the quadratic potential as in the previous example of one rod. $V(\mathbf{x}) = \mathbf{x}^T K \mathbf{x} / 2$. Here $K = \text{diag}\{\mu_1, \mu_2, \mu_3\}$, where $\mu_1 < \mu_2 < \mu_3$. Next, we show the following property of the drift flow of (5.6) on $\mathbb{S}^2 \times \mathbb{S}^2$ for the weak strength of the interaction.

PROPOSITION 2. *If the coupling constant A in the potential equation (5.7) satisfies*

$$(5.9) \quad A < \frac{1}{4} \min_{i \neq j} |\mu_i - \mu_j|,$$

then all fixed points of the deterministic drift flow of (5.6) are the 36 points

$$(\pm \mathbf{e}_i, \pm \mathbf{e}_j), \quad i, j = 1, 2, 3,$$

where \mathbf{e}_i is the unit eigenvector of K for eigenvalue μ_i , for instance, $\mathbf{e}_1 = (1, 0, 0)$. Moreover, the four points $(\pm \mathbf{e}_1, \pm \mathbf{e}_1)$ are stable (classified as sink), the four points $(\pm \mathbf{e}_3, \pm \mathbf{e}_3)$ are unstable (classified as source), and other fixed points are all saddles.

Proof. It can be verified that any fixed point $(\mathbf{x}_1, \mathbf{x}_2)$ must satisfy the following equations:

$$(5.10) \quad -K\mathbf{x}_1 + 2A\langle \mathbf{x}_1, \mathbf{x}_2 \rangle \mathbf{x}_2 - 2A\langle \mathbf{x}_1, \mathbf{x}_2 \rangle^2 \mathbf{x}_1 + (\mathbf{x}_1^\top K \mathbf{x}_1) \mathbf{x}_1 = 0,$$

$$(5.11) \quad -K\mathbf{x}_2 + 2A\langle \mathbf{x}_1, \mathbf{x}_2 \rangle \mathbf{x}_1 - 2A\langle \mathbf{x}_1, \mathbf{x}_2 \rangle^2 \mathbf{x}_2 + (\mathbf{x}_2^\top K \mathbf{x}_2) \mathbf{x}_2 = 0,$$

$$(5.12) \quad \|\mathbf{x}_1\| = \|\mathbf{x}_2\| = 1.$$

If $\langle \mathbf{x}_1, \mathbf{x}_2 \rangle = 0$, (5.10) and (5.11) suggest \mathbf{x}_1 and \mathbf{x}_2 must be unit eigenvectors of K corresponding to distinctive eigenvalues, respectively. It gives 24 fixed points $(\pm \mathbf{e}_i, \pm \mathbf{e}_j)$ for $i \neq j$ in this case.

If $\langle \mathbf{x}_1, \mathbf{x}_2 \rangle \neq 0$, (5.10) and (5.11) together imply that $\langle \mathbf{x}_1, \mathbf{x}_2 \rangle (\mathbf{x}_1^\top K \mathbf{x}_1 - \mathbf{x}_2^\top K \mathbf{x}_2) = 0$, or, $\mathbf{x}_1^\top K \mathbf{x}_1 = \mathbf{x}_2^\top K \mathbf{x}_2 = \lambda$. Furthermore, by considering (5.10) \pm (5.11), we have $\mathbf{x}_1 \pm \mathbf{x}_2$ are either zero vector or an eigenvector of K . The former case gives the other 12 fixed points $(\pm \mathbf{e}_i, \pm \mathbf{e}_i)$. The latter case that $\mathbf{x}_1 \pm \mathbf{x}_2$ is an eigenvector of K will eventually lead to an equality $\mu_i - \mu_j = 4A\langle \mathbf{x}_1, \mathbf{x}_2 \rangle$. But since it follows $|\mu_i - \mu_j| = |4A\langle \mathbf{x}_1, \mathbf{x}_2 \rangle| \leq 4A\|\mathbf{x}_1\|\|\mathbf{x}_2\| = 4A$, which contradicts condition (5.9), there are no other solutions.

The conclusions of the linear stability are based on the calculation of the Jacobian matrices at these fixed points. We neglect the details. \square

In all, there are 36 different fixed points. From the above proof we know that $(\mathbf{e}_i, \mathbf{e}_j)$ is a fixed point even without the condition (5.9). If the condition (5.9) does not hold, there may be other fixed points and it can be shown that there are at most 60 fixed points. In our numerical calculations, we choose $K = \text{diag}\{1, 3, 5\}$, $A = 0.4$ to satisfy the condition (5.9). In addition, we always let $\sigma_1 = 1$ but allow σ_2 to vary.

The transition path we will study is from the initial state $(\mathbf{e}_1, -\mathbf{e}_1)$ to the final state $(-\mathbf{e}_1, \mathbf{e}_1)$, in which both rods flip over their initial directions. Since the initial and final states both lie in the \mathbf{e}_1 - \mathbf{e}_2 plane for each rod, then by symmetry consideration, the transition paths, i.e., the minimizers of the action functional (5.8), must also lie in this plane. Our numerical calculations based on $\mathbb{S}^2 \times \mathbb{S}^2$ indeed verify this fact. Therefore, we can visualize the obtained paths and interpret our results on a lower-dimensional product space $\mathbb{S}^1 \times \mathbb{S}^1$. It is convenient to use local coordinates $(\theta_1, \theta_2) \in [0, 2\pi) \times [0, 2\pi)$ to denote a point of the path (ϕ_1, ϕ_2) :

$$\phi_1 = [\cos \theta_1, \sin \theta_1, 0], \quad \phi_2 = [\cos \theta_2, \sin \theta_2, 0].$$

In this local coordinates representation, the initial and final states $(\mathbf{e}_1, -\mathbf{e}_1)$ and $(-\mathbf{e}_1, \mathbf{e}_1)$ can be written as $(\theta_1, \theta_2) = (0, \pi)$ and $(\pi, 0)$, respectively. There are 16 fixed points on $\mathbb{S}^1 \times \mathbb{S}^1$ in total. Further taking into account the spatial symmetry, we only need to focus on four sinks and five saddles for $(\theta_1, \theta_2) \in [0, \pi] \times [0, \pi]$, as shown in Table 1 and Figure 7. In the figure, the heteroclinic orbits between these fixed points are shown in arrowed lines. The saddle point sa_5 , at the center of the figure, is on the separatrix of all four sinks in the phase space and its unstable manifold has dimension 2. All four other saddle points have one dimensional unstable manifold for each, i.e., they are index-1 saddles.

TABLE 1
 Four sinks and five saddles for $(\theta_1, \theta_2) \in [0, \pi] \times [0, \pi]$.

Stable points	$\mathbb{S}^2 \times \mathbb{S}^2$	(θ_1, θ_2)	Saddle points	$\mathbb{S}^2 \times \mathbb{S}^2$	(θ_1, θ_2)
si_1	$(\mathbf{e}_1, \mathbf{e}_1)$	$(0, 0)$	sa_1	$(\mathbf{e}_2, \mathbf{e}_1)$	$(\pi/2, 0)$
si_2	$(\mathbf{e}_1, -\mathbf{e}_1)$	$(0, \pi)$	sa_2	$(\mathbf{e}_1, \mathbf{e}_2)$	$(0, \pi/2)$
si_3	$(-\mathbf{e}_1, \mathbf{e}_1)$	$(\pi, 0)$	sa_3	$(\mathbf{e}_2, -\mathbf{e}_1)$	$(\pi/2, \pi/2)$
si_4	$(-\mathbf{e}_1, -\mathbf{e}_1)$	(π, π)	sa_4	$(-\mathbf{e}_1, \mathbf{e}_2)$	$(\pi, \pi/2)$
			sa_5	$(\mathbf{e}_2, \mathbf{e}_2)$	$(\pi/2, \pi/2)$

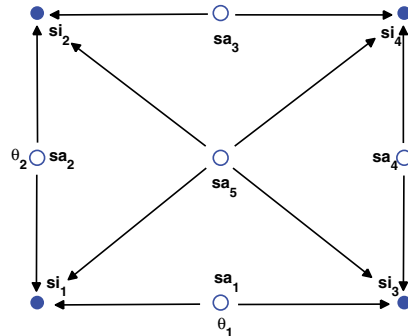


FIG. 7. Fixed points in θ_1 - θ_2 plane. Sinks are denoted by solid dots (\bullet), saddles are denoted by circles (\circ). The arrows shows the heteroclinic orbits of the deterministic drift flow. All saddles have index 1, except sa_5 has index 2.

The transition path we studied is from si_2 to si_3 , two diagonal nodes in Figure 7. In solving minimization problem $\inf_{\phi} \hat{S}[\phi]$, one critical issue is how to locate the global solution rather than being trapped by the local ones. Since there is no efficient global minimization solvers (we used the MATLAB subroutine `fmincon` for nonlinear optimization), the selection of initial guess of path is crucial. We utilize the information of the heteroclinic orbits in Figure 7 and propose the following five routes as our initial guesses by choosing different fixed points as intermediate states:

- A. $si_2 \rightarrow sa_5 \rightarrow si_3$,
- B. $si_2 \rightarrow sa_2 \rightarrow sa_5 \rightarrow si_3$,
- C. $si_2 \rightarrow sa_2 \rightarrow si_1 \rightarrow sa_1 \rightarrow si_3$,
- D. $si_2 \rightarrow sa_3 \rightarrow sa_5 \rightarrow si_3$,
- E. $si_2 \rightarrow sa_3 \rightarrow si_4 \rightarrow sa_4 \rightarrow si_3$.

Then, each choice of initial guess gives a local minimum action path and the obtained minimized actions for the five solutions are plotted in Figure 8. The lowest value of these five curves gives the global minimum action.

When $\sigma_1 = \sigma_2$, the same global solution can be achieved from initial guesses A, B, and D. This global minimum action path is the diagonal line ($si_2 \rightarrow sa_5 \rightarrow si_3$) in the θ_1 - θ_2 visualization (Figure 9(a)). However, when $\sigma_2 \neq \sigma_1$, the symmetric path ($si_2 \rightarrow sa_5 \rightarrow si_3$) is not the global minimal solution; in fact, the path for the global solution will pass through index-1 saddle point sa_2 (if $\sigma_2 > \sigma_1$) or sa_3 (if $\sigma_2 < \sigma_1$).

Take $\sigma_2 = 1.2 > \sigma_1 = 1$ as an example. The transition path corresponding to the global minimizer of the action functional is shown in the right panel of Figure 9(b). The symmetry of the transition path is broken for this case of unequal diffusion coefficients. This asymmetric path has three segments and accordingly the transition process can be understood via three stages. The first stage is from $si_2 = (\mathbf{e}_1, -\mathbf{e}_1)$

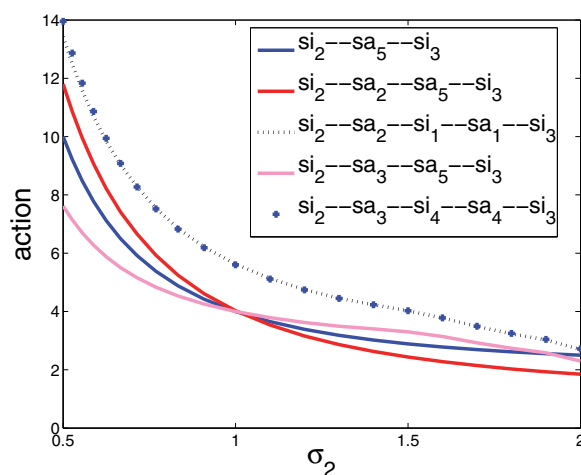


FIG. 8. Numerical values of the minimal actions corresponding to five different initial guess paths by varying the diffusion coefficient σ_2 .

to $sa_2 = (e_1, e_2)$, where the first rod does not move much and only the second rod, which has the larger diffusion coefficient, rotates clockwise to the vertical position e_2 ; then, at the second stage, which is from sa_2 to $sa_5 = (e_2, e_2)$, the second rod is almost still and “waits” in the state e_2 for the first rod to move from e_1 to e_2 . Once both rods reach the saddle state sa_5 , the last state starts and both rods directly approach the final state si_3 following the heteroclinic orbit in Figure 7 without any aid from noise.

The above numerical results demonstrate a selection mechanism: the rod with a larger diffusion coefficient σ is subject to large random perturbations with the same white noise realizations, and thus it is easier to make transition movements first. We may call this rod as an “active” rod. After this rod actively approaches a critical state (e_2 here), it rests there, and the interaction $U(\mathbf{x}_1, \mathbf{x}_2)$ starts to be the main contributor to influence the system and the previously still rod (“passive” one) is attracted by U from the active rod to the critical state, from where the entire system has crossed all the barriers on the route of the transition. What is unexpected here is that the two rods move in tandem during the first and second transition stages. Taking an analogy of the so-called reaction coordinate in chemical reactions, we can think of θ_2 as an excellent candidate for reaction coordinate at the first transition stage and θ_1 at the second stage. When we varied σ_2 from 1 to 2 ($\sigma_1 = 1$ is fixed), the numerical result shows the robustness of this set of reaction coordinates especially at the first stage from si_2 to sa_2 . Refer to Figure 9(c) for the plots of 40 (global minimum action) paths for various values of σ_2 by equally dividing the σ_2^2 from 1 to 4.

In all, when the diffusion coefficients for the two rigid rods are identical, the transition path is symmetric and both rods move simultaneously in the transitions. If one of the diffusion coefficients is adjusted, then the rod molecule with the larger diffusion amplitude will initiatively move into some intermediate state. Only after this step will the other rod follow the movement in a similar fashion. The unbalance of the noise amplitudes triggers an ordered process for each rod to make the transitions.

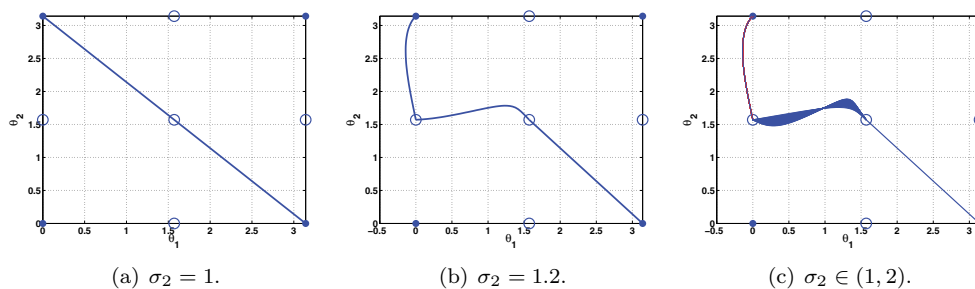


FIG. 9. Global minimum action path(s) from si_2 to si_3 .

6. General bead-rod systems. We have studied the most probable transition pathway for the stochastic dynamics with explicitly known projection operators. In the theory of polymeric fluids, people are also interested in the stochastic conformational dynamics of the bead-rod system [5] with Lagrange multipliers as we discussed in section 3.1. All of our derivations before can be applied in this special case. Let us illustrate this point concretely as below.

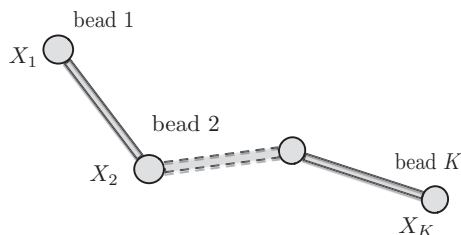


FIG. 10. The schematics of the bead-rod polymer chain with K beads.

Consider a bead-rod polymer chain with K -beads (Figure 10), being described, for instance, by the following over-damped stochastic dynamics:

$$(6.1) \quad d\mathbf{X}_i = \left(\mathbf{u}(\mathbf{X}_i) + (T_i \mathbf{n}_i - T_{i-1} \mathbf{n}_{i-1}) \right) dt + \sqrt{\varepsilon} d\mathbf{W}_i, \quad i = 1, 2, \dots, K,$$

where \mathbf{X}_i is the \mathbb{R}^3 coordinate of the i th bead, $\mathbf{u}(\mathbf{X})$ is the drift part which includes the effect of fluid velocity and driving potential at \mathbf{X} , $\mathbf{n}_i = (\mathbf{X}_{i+1} - \mathbf{X}_i) / \|\mathbf{X}_{i+1} - \mathbf{X}_i\|$ for $i = 1, 2, \dots, K - 1$, and T_i is the tension between the beads i and $i + 1$ such that the constraints

$$(6.2) \quad \|\mathbf{X}_{i+1} - \mathbf{X}_i\| = 1, \quad i = 1, 2, \dots, K - 1,$$

are satisfied. We take the convention that $T_0 = 0$ and $\mathbf{n}_K = 0$. It is obvious that the tension $\{T_i\}$ plays the role of the Lagrange multipliers which will be determined by the constraints (6.2).

Mathematically, (6.1) in engineering literature is not well-defined since the tension force T_i will involve the white noise \mathbf{W}_i as singular forces. Indeed, it can be perfectly put into the framework shown in Proposition 1 with the constraints

$$c_j(\mathbf{x}) := \frac{1}{2} (\|\mathbf{x}_{j+1} - \mathbf{x}_j\|^2 - 1), \quad j = 1, \dots, K - 1,$$

and the relation between Lagrange multipliers:

$$d\mu_j = -T_j dt, \quad j = 1, \dots, K,$$

where $\mathbf{x} = (\mathbf{x}_1, \dots, \mathbf{x}_K) \in \mathbb{R}^{3K}$. With this connection, (6.1) is transformed to

$$(6.3) \quad d\mathbf{X} = \Pi(\mathbf{u}(\mathbf{X})dt + \circ\sqrt{\varepsilon}d\mathbf{W}),$$

where $\mathbf{X} = (\mathbf{X}_1, \dots, \mathbf{X}_K)$, $\mathbf{W} = (\mathbf{W}_1, \dots, \mathbf{W}_K)$, and the matrix $\Pi = I - G^T M^{-1} G$ is an orthogonal projection as defined in Proposition 1. This formulation will be particularly useful to design the projection type methods for the SDE (6.1). It is also interesting to observe that the SDE (6.3) has an equivalent form

$$(6.4) \quad d\mathbf{X} = \left(\mathbf{u}(\mathbf{X}) + \sum_{j=1}^{K-1} \mu_j^r \nabla c_j(\mathbf{X}) \right) dt + \Pi \circ \sqrt{\varepsilon} d\mathbf{W}$$

or

$$(6.5) \quad d\mathbf{X} = \Pi \left[\left(\mathbf{u}(\mathbf{X}) + \sum_{j=1}^{K-1} \mu_j^r \nabla c_j(\mathbf{X}) \right) dt + \circ\sqrt{\varepsilon} d\mathbf{W} \right],$$

where $\mu^r(\mathbf{x}) = -M^{-1}G\mathbf{u}(\mathbf{x})$ is the “regular” part of the Lagrange multipliers including only the drift.

Thanks to the result (C.5) in Appendix C, we have the Freidlin–Wentzell action functional to the SDE (6.3) as

$$(6.6) \quad S_T[\phi] = \frac{1}{2} \int_0^T \|\dot{\phi} - \Pi\mathbf{u}(\phi)\|^2 dt$$

subject to the constraints

$$\phi \in \mathcal{M} = \left\{ \phi \mid c_j(\phi) = 0, \quad j = 1, \dots, K-1 \right\} \quad \text{and} \quad \dot{\phi} \in T_\phi \mathcal{M}.$$

Its geometric action functional has the form based on the result (3.27)

$$\hat{S}[\varphi] = \int_0^1 \|\varphi'\| \|\Pi\mathbf{u}\| - \langle \varphi', \Pi\mathbf{u} \rangle d\alpha$$

subject to the constraints $\varphi' \in T_\varphi \mathcal{M}$.

Based on the obtained optimization problem with constraints or its relaxation form, we can compute the transition pathways correspondingly. We shall not develop the study on this point here since it is beyond the main goal of this paper. Further research on this topic will be a future study.

7. Summary. In this summary, we want to reiterate the mathematical importance of specifying how the constrained dynamical system is perturbed by noise when one intends to investigate the transition paths in these constrained systems. Here we considered the SDE whose solution satisfies constraints, i.e., stays on \mathcal{M} , for any ε , rather than accommodates for constraints in the asymptotic sense. The asymptotic limit $\varepsilon \downarrow 0$ is only applied in the large deviation result. In formulating the action

functional, we took the approach of using the local projection Π to describe the constraints and solved the issue of degeneracy brought by this projection operator in the augmented Euclidean space \mathbb{R}^n .

In the reversible case where the drift term is of gradient type and the diffusion coefficient is an isotropic constant, we proved that the constraints actually do not bring significant numerical difficulties and the original string method still works by using the projected gradient force for each image on string: It is essentially the same as solving the deterministic gradient flow on the manifold.

In the irreversible case, one needs to pay attention to the generalized inverse of the projection operator in the calculation of constrained minimum action. The state-dependent Π_x^{-1} term appears in the action functional and the path calculation. In our current version of the constrained minimum action method and for all examples in this paper, we assume that Π and Π^{-1} as well as their derivatives are all analytically available. It may be rewarding to explore the numerically convenient extension of b and \tilde{a} on \mathcal{M} to the nonunique Π , a and b in \mathbb{R}^n in order to achieve a new form of Π^{-1} that is easier to compute. We leave this idea to a future study. Additionally, the resulting constrained optimization problem needs to be solved by good initial guesses to find the global solution. The initial guesses in our example of rigid rod models are built on some prior understanding of the phase spaces. For the numerical results, when the liquid crystal molecules are influenced by macroscopic fluid or unequal diffusion coefficients, the global minimum action pathway we found here reveals very interesting nonequilibrium phenomena, and these phenomena are believed to be generic in irreversible systems and deserve further investigation.

Appendix A.

Proof of Theorem 1. By Ito’s formula and the constraint conditions, we have

$$0 = dc_j(X) = (\nabla c_j(X))^T dX + \frac{1}{2} \nabla^2 c_j(X) : (dX dX^T).$$

Comparing the terms involving Brownian motion, we get

$$GG^T \beta + G\sigma = 0,$$

which implies (3.6). The terms involving dt yield to

$$G(b + G^T \alpha) + \frac{1}{2} \nabla^2 c : (BB^T) = 0,$$

which gives (3.5).

Substituting β into (3.3) and (3.4), we obtain

$$(A.1) \quad dX = \left(b(X) + G^T \alpha(X) \right) dt + P\sigma(X) dW.$$

Notice that $P^T = P$ and $GP = 0$, then

$$P^2 = I - 2G^T M^{-1} G + G^T M^{-1} G G^T M^{-1} G = P.$$

This implies that P is the orthogonal projection to $T\mathcal{M}$.

To prove (3.8), from (A.1) we note

$$(A.2) \quad dX = \left(b(X) + G^T \alpha(X) \right) dt + \left(P\sigma(X) dW - P\sigma(X) \circ dW \right) + P\sigma(X) \circ dW.$$

From the relation between Ito and Stratonovich integrals, we have

$$\begin{aligned}
& \left(P\sigma(X) \circ dW - P\sigma(X) dW \right)_i = \frac{1}{2} \sum_{j,k} \partial_k (P\sigma)_{ij} (P\sigma)_{kj} dt \\
& = \frac{1}{2} \sum_{j,k} \partial_k \left(e_i^\top P\sigma e_j \right) e_k^\top P\sigma e_j dt = -\frac{1}{2} e_i^\top \sum_{j,k} \partial_k \left(G^\top M^{-1} G\sigma e_j \right) e_k^\top P\sigma e_j dt \\
& = -\frac{1}{2} e_i^\top \sum_{j,k} (\partial_k G^\top) M^{-1} G\sigma e_j e_k^\top P\sigma e_j dt - \frac{1}{2} e_i^\top G^\top \sum_{j,k} \partial_k \left(M^{-1} G\sigma \right) e_j e_k^\top P\sigma e_j dt \\
& =: (F_1)_i dt + (F_2)_i dt,
\end{aligned}$$

where e_i , e_j , and e_k are canonical basis vectors in the corresponding Euclidean space, and the partial derivative of a matrix is defined to take the differential to each component. F_1 actually vanishes if we assume $\sigma\sigma^\top$ is a scalar matrix:

$$\begin{aligned}
F_1 & = -\frac{1}{2} \sum_{j,k} (\partial_k G^\top) M^{-1} G\sigma e_j e_k^\top P\sigma e_j = -\frac{1}{2} \sum_{j,k} (\partial_k G^\top) M^{-1} G\sigma e_j e_j^\top \sigma^\top P e_k \\
& = -\frac{1}{2} \sum_k (\partial_k G^\top) M^{-1} G\sigma\sigma^\top P e_k = -\frac{1}{2} \theta \sum_k (\partial_k G^\top) M^{-1} G P e_k = 0,
\end{aligned}$$

where the last equality comes from $GP = 0$. The expression for F_2 can be denoted as $F_2 = G^\top \gamma$ for some vector γ . Substituting this form into (A.2), we get

$$dX = \left(b(X) + G^\top (\alpha(X) - \gamma(X)) \right) dt + P\sigma(X) \circ dW.$$

From $dc_j(X) = (\nabla c_j(X))^\top \circ dX = 0$, i.e., $G \circ dX = 0$, we obtain

$$Gb(X) + GG^\top (\alpha(X) - \gamma(X)) = 0.$$

This means that $\alpha(X) - \gamma(X) = -M^{-1}Gb(X)$. So (3.8) holds. \square

Appendix B. Projection operator and its inverse. From the constraint $\Pi u = y - \Pi b(x)$ for the minimization problem (3.19), one may formally view u as an element in the set $\Pi^{-1}(y - \Pi b(x))$ which has the minimal a -norm. To ease the presentation, we redefine Π^{-1} as follows.

DEFINITION 1. *Let Π be an orthogonal projection matrix in \mathbb{R}^n and the diffusion matrix a be a positive definite matrix. For any $v \in \text{Img}(\Pi)$, we define $\Pi^{-1}v$ as the vector $u^* \in \mathbb{R}^n$ such that u^* solves $\min_{\Pi u=v} \|u\|_a$.*

The above defined $\Pi^{-1}v$ for a given $v \in \text{Img}(\Pi)$ is unique since a is not singular. Π^{-1} is a linear transformation defined on $\text{Img}(\Pi)$. We point out that Π^{-1} is not an inverse of Π in the usual sense because although $\Pi \circ \Pi^{-1}$ is identity restricted on the space $\text{Img}(\Pi)$, it is generally invalid that $\Pi^{-1}(\Pi v) = v$. This generalized inverse $\Pi^{-1} : \text{Img}(\Pi) \rightarrow \mathbb{R}^n$ depends on the metric induced by a . If $a(x)$ is a scalar matrix and Π is orthogonal projections, then Definition 1 directly shows that Π^{-1} is identity restricted on $\text{Img}(\Pi)$.

We next point out some useful properties of Π^{-1} and the connection to \tilde{a} -norm. Two examples of the manifold cases are also shown for illustration.

PROPOSITION 3. $\Pi^{-1} = a\Pi^T \tilde{a}^{-1}$. If $\Pi = \Pi^T$, then $\Pi^{-1} = a\tilde{a}^{-1}$ and $\tilde{a}^{-1} = a^{-1}\Pi^{-1}$.

Proof. The proof is straightforward from the proof of Proposition 1. \square

PROPOSITION 4. *If $v \in \text{Img}(\Pi)$, then*

$$(B.1) \quad \|v\|_{\tilde{a}} = \|\Pi^{-1}v\|_a.$$

In addition, for v_1, v_2 both in $\text{Img}(\Pi)$,

$$(B.2) \quad \langle v_1, v_2 \rangle_{\tilde{a}} = \langle v_1, \Pi^{-1}v_2 \rangle_a = \langle v_1, \Pi^{-1}v_2 \rangle_a.$$

Proof. (B.1) is Proposition 1. For the second part, $\langle v_1, v_2 \rangle_{\tilde{a}} = \langle v_1, \tilde{v}_2 \rangle = \langle \Pi v_1, \tilde{v}_2 \rangle = \langle v_1, \Pi^T \tilde{v}_2 \rangle = \langle v_1, a^{-1} \Pi^T \tilde{v}_2 \rangle_a = \langle v_1, \Pi^{-1}v_2 \rangle_a$. \square

PROPOSITION 5. *For every $w \in \text{Ker}(\Pi)$ and $v \in \text{Img}(\Pi)$, we have*

$$\langle \Pi^{-1}v, w \rangle_a = 0.$$

Proof. Let $u^* = \Pi^{-1}v$. Define $u_\theta = u^* + \theta w \forall \theta \in \mathbb{R}$. Then $\Pi u_\theta = \Pi u^* = v \forall \theta$. So, the function $f(\theta) := \|u_\theta\|_a^2$ has a minimal value $\|u^*\|_a^2$ at $\theta_0 = 0$. Consequently, $f'(\theta_0) = 0$ and $\langle u^*, w \rangle = 0$ follows. \square

PROPOSITION 6. *For any vector $v \in \text{Img}(\Pi)$, it is true that*

$$\begin{aligned} \|\Pi^{-1}v\|_a^2 &= \langle v, \Pi^{-1}v \rangle_a, \\ \|v\|_a^2 &= \|\Pi^{-1}v\|_a^2 + \|v - \Pi^{-1}v\|_a^2. \end{aligned}$$

Proof. The first equality is due to the fact $v - \Pi^{-1}v \in \text{Ker}(\Pi)$ and Proposition 5. Then it follows that $\|v\|_a^2 = \langle v, \Pi^{-1}v \rangle_a + \langle v, v - \Pi^{-1}v \rangle_a = \|\Pi^{-1}v\|_a^2 + \langle v, v - \Pi^{-1}v \rangle_a$. Since $\langle \Pi^{-1}v, v - \Pi^{-1}v \rangle_a = 0$ due to Proposition 5, then $\|v\|_a^2 = \|\Pi^{-1}v\|_a^2 + \|v - \Pi^{-1}v\|_a^2$. \square

PROPOSITION 7. *If $\dim \text{Ker}(\Pi) = K$, and $\text{Ker}(\Pi) = \text{span}\{\xi_k : k = 1, \dots, K\}$, then for any $v \in \text{Img}(\Pi)$,*

$$\|v\|_a^2 = \|\Pi^{-1}v\|_a^2 + \|\hat{v}\|_M^2 = \|v\|_{\tilde{a}}^2 + \|\hat{v}\|_M^2,$$

where $M = (M_{ij}) = \langle \xi_i, \xi_j \rangle_a$, $i, j = 1, 2, \dots, K$, and $\hat{v} = (\hat{v}_k) = \langle v, \xi_k \rangle_a$, $k = 1, \dots, K$.

When a is a scalar matrix, i.e., the condition (3.7) holds, and $\Pi = \Pi^T$, then $\|v\|_a^2 = \|v\|_{\tilde{a}}^2$, i.e., a -norm and \tilde{a} -norm are identical.

Proof. Write $v - \Pi^{-1}v = \sum_k \lambda_k \xi_k$; then these λ_k minimize $\|v - \sum_k \lambda_k \xi_k\|_a^2$. So, $\lambda = (\lambda_1, \lambda_2, \dots, \lambda_K)^T$ satisfy $M\lambda = \hat{v}$. Note that $\|v - \Pi^{-1}v\|_a^2 = \|\sum_k \lambda_k \xi_k\|_a^2 = \lambda^T M \lambda = \hat{v}^T M^{-1} \hat{v} = \|\hat{v}\|_M^2$. The conclusion is then immediate from Proposition 6.

When $\Pi = \Pi^T$, $\text{ker}(\Pi)$ is orthogonal to $\text{Img}(\Pi)$ in \mathbb{R}^n . If furthermore $a(x)$ is scalar, then by (3.7), $\langle v, \xi_k \rangle_a = \langle v, \xi_k \rangle / \theta(x) = 0$. \square

When Π is the orthogonal projection induced by the constraints $\{c_k(x) = 0 : k = 1, 2, \dots, n - d\}$, then the basis of $\text{Ker}(\Pi)$ above can be chosen as $\xi_k = \nabla c_k(x)$. In the following, we show calculations of \tilde{a}^{-1} and Π^{-1} for two simple examples.

Example 2 (planar projection). Consider a hyperplane in \mathbb{R}^n , $\mathcal{M} = \{x = (x_1, x_2, \dots, x_n) : x_n = 0\}$, corresponding to the unique constraint $c(x) = x_n = 0$. Then the (orthogonal) projection $\Pi = \begin{bmatrix} I_{n-1} & 0 \\ 0 & 0 \end{bmatrix}$. Write $a = \begin{bmatrix} A_{11} & A_{12} \\ A_{12} & A_{22} \end{bmatrix}$, where A_{11} has size $(n - 1) \times (n - 1)$. Then $v \in \text{Img}(\Pi)$ has the form $v = (v_1, 0)^T$, where v_1 has size $n - 1$. It is easy to calculate that

$$\tilde{a} = \Pi a \Pi^T = \begin{bmatrix} A_{11} & 0 \\ 0 & 0 \end{bmatrix},$$

$$\tilde{a}^{-1}v = \begin{bmatrix} A_{11}^{-1}v_1 \\ 0 \end{bmatrix} = \begin{bmatrix} A_{11}^{-1} & * \\ 0 & * \end{bmatrix} v,$$

and

$$\Pi^{-1}v = a\tilde{a}^{-1}v = \begin{bmatrix} A_{11} & A_{12} \\ A_{12}^T & A_{22} \end{bmatrix} \begin{bmatrix} A_{11}^{-1}v_1 \\ 0 \end{bmatrix} = \begin{bmatrix} A_{11}^{-1}v_1 \\ A_{12}^T A_{11}^{-1}v_1 \end{bmatrix} = \begin{bmatrix} A_{11}^{-1} & * \\ A_{12}^T A_{11}^{-1} & * \end{bmatrix} v.$$

Example 3 (spherical projection). Consider the spherical case $\mathcal{M} = \mathbb{S}^d$, where $d = n - 1$. The constraint function is $c(x) = \|x\|^2 - 1 = 0$. The projection onto the tangent space is $\Pi_x = I - \mathbf{n}(x) \otimes \mathbf{n}(x)$, where $\mathbf{n}(x) = x/\|x\|$ is the unit (L^2 -norm) normal. The kernel space $\text{Ker}(\Pi_x) = \text{span}\{\mathbf{n}(x)\}$. The calculation shows that for any $v \in \text{Img}(\Pi)$

$$\Pi^{-1}v = v - \frac{\langle v, \mathbf{n} \rangle_a}{\langle \mathbf{n}, \mathbf{n} \rangle_a} \mathbf{n} = v - \langle v, \mathbf{n}_a \rangle_a \mathbf{n}_a$$

and

$$\tilde{a}^{-1}v = a^{-1}v - \langle v, \mathbf{n}_a \rangle_a a^{-1}\mathbf{n}_a,$$

where $\mathbf{n}_a = \mathbf{n}/\|\mathbf{n}\|_a$ is the unit vector in sense of a -norm.

Appendix C. Euler–Lagrange equations and related discussions. In summary, the action functional for the SDE (3.13) is

$$(C.1) \quad S_T^{\mathcal{M}}[\phi] = \begin{cases} \inf_u \left\{ \frac{1}{2} \int_0^T \|u\|_a^2 dt : \dot{\phi} - \Pi b(\phi) = \Pi u, \right\} & \text{if } \phi \in \mathcal{A}, \\ +\infty & \text{otherwise.} \end{cases}$$

In (C.1), u is a function of t and is equal to $\Pi^{-1}(\dot{\phi} - \Pi b(\phi))$ for $t \in [0, T]$ by Definition 1. Then the action functional (C.1) (for finite value) is written in terms of Π^{-1} as

$$(C.2) \quad S_T^{\mathcal{M}}[\phi] = \frac{1}{2} \int_0^T \left\| \Pi^{-1}(\dot{\phi} - \Pi b(\phi)) \right\|_a^2 dt,$$

which is defined over the admissible set \mathcal{A} or the equivalent \mathcal{A}' . By Proposition 2, (C.2) is also equivalent to

$$(C.3) \quad S_T^{\mathcal{M}}[\phi] = \frac{1}{2} \int_0^T \left\| \dot{\phi} - \tilde{b}(\phi) \right\|_{\tilde{a}}^2 dt.$$

In other words, (C.1), (C.2), and (C.3), are three equivalent forms of the action functional.

In the following, we want to compare the action (C.2) or (C.3) to the action for the following SDE in the ambient space without the projection of the random forcing term, i.e.,

$$(C.4) \quad dX = (\Pi b(X)) dt + \sqrt{\varepsilon} \sigma(X) dW,$$

whose solution X_t is not exactly on \mathcal{M} . The action for (C.4) is

$$(C.5) \quad S_T^1[\phi] := \frac{1}{2} \int_0^T \left\| \dot{\phi} - \Pi b(\phi) \right\|_a^2 dt \quad \forall \phi \in AC([0, T], \mathbb{R}^n).$$

Another case we want to compare with is the action for the SDE $dX = b(X) dt + \sqrt{\varepsilon}\sigma(X) dW$ in \mathbb{R}^n ,

$$(C.6) \quad S_T^0[\phi] := \frac{1}{2} \int_0^T \|\dot{\phi} - b(\phi)\|_a^2 dt \quad \forall \phi \in AC([0, T], \mathbb{R}^n).$$

This action functional (C.6) probably looks far from a constrained problem. But is it possible that only in the last stage imposing the constraints for the action functional, S_T^0 and S_T^1 give the same minimizing path, as the constrained string method [6] works for gradient systems? We shall offer counterexamples to show that all three functionals in general have *different* minimizers by analyzing the Euler–Lagrange equations for these functionals. We also give Remark 4 below to justify the constrained string method proposed in [6].

To be specific, we consider the following three constrained optimization problems:

$$(P0) \quad \inf_{\phi \in \mathcal{A}} S^0[\phi] = \inf_{\phi \in \mathcal{A}} \frac{1}{2} \int_0^T \|\dot{\phi} - b(\phi)\|_a^2 dt,$$

$$(P1) \quad \inf_{\phi \in \mathcal{A}} S^1[\phi] = \inf_{\phi \in \mathcal{A}} \frac{1}{2} \int_0^T \|\dot{\phi} - \Pi b(\phi)\|_a^2 dt,$$

$$(P*) \quad \inf_{\phi \in \mathcal{A}} S^{\mathcal{M}}[\phi] = \inf_{\phi \in \mathcal{A}} \frac{1}{2} \int_0^T \|\dot{\phi} - \tilde{b}(\phi)\|_{\tilde{a}}^2 dt.$$

For (P0) and (P1), the constraint $\phi \in \mathcal{A}$, i.e., $\phi(t) \in \mathcal{M}$ is the forced constraint. But for (P*), \mathcal{A} is the domain for $S^{\mathcal{M}}$. We shall prove that the minimizing paths for these three problems (P0), (P1), (P*), are generally not the same. The approach is to study their Euler–Lagrange equations.

With the assumption for the state-independent diffusion a , we have for (P0), $-\frac{\delta S^0}{\delta \phi}[\phi] = \dot{p} + J^T(\phi)p$ in $L^2([0, T], \mathbb{R}^n)$ space, where $p(t) = a^{-1}(\dot{\phi} - b(\phi))$, $J(x) = \nabla b(x)$, $J_{ij} = \frac{\partial b_i}{\partial x_j}$. Thus the Euler–Lagrange equation in the constraint space $L^2([0, T], \mathcal{M})$, which the minimizer path for (P0) must satisfy, is

$$(C.7) \quad \Pi^T (\dot{p} + J^T(\phi)p) = 0.$$

Similarly, the Euler–Lagrange equation for (P1) is

$$(C.8) \quad \Pi^T (\dot{p} + \tilde{J}^T(\phi)p) = 0,$$

where $p(t) := a^{-1}(\dot{\phi} - \tilde{b}(\phi))$, $\tilde{J}(x) := \nabla \tilde{b}(x) = \nabla(\Pi_x b(x))$.

For (P*), the Euler–Lagrange equation is

$$(C.9) \quad -\frac{\delta S^{\mathcal{M}}}{\delta \phi} = \dot{\tilde{p}} + \tilde{J}^T \tilde{p} - \frac{1}{2}(\tilde{a}\tilde{p}) \otimes (\tilde{a}\tilde{p}) : \nabla(\tilde{a}^{-1})$$

for $\phi \in \mathcal{A}$, where $\tilde{p} := \tilde{a}^{-1}(\dot{\phi} - \tilde{b})$, the tensor contraction $(y \otimes y : D)_k := \sum_{ijk} y_i y_j D_{ijk}$ with $D = \nabla(\tilde{a}^{-1})$, $D_{ijk} = \frac{\partial}{\partial x_k}(\tilde{a}^{-1})_{ij}$.

PROPOSITION 8. *In general, the solution of the Euler–Lagrange equation for (P0) is not equivalent to the solution of the Euler–Lagrange equation for (P1). Therefore, the minimizing paths for (P0) and (P1) are different.*

Proof. We consider a simple case that $\Pi_x \equiv \Pi \forall x \in \mathcal{M}$ and $\Pi = \Pi^T$ (for instance, Example 2). Assume $a(x) \equiv I$ and $b(x) = -\nabla V(x)$ (gradient system).

Thus, $J(x) = J(x)^\top = -\nabla^2 V(x)$, $\tilde{J} = \Pi J$, $\tilde{J}^\top = J\Pi$. Let ϕ_0 and ϕ_1 satisfy the Euler–Lagrange equation for (P0) and (P1), respectively. Then

$$\Pi \left(\ddot{\phi}_0 - J(\phi_0)b(\phi_0) \right) = 0$$

and

$$\Pi \left(\ddot{\phi}_1 - J(\phi_1)\Pi b(\phi_1) \right) = 0.$$

In general, $\Pi J b$ is not equal $\Pi J \Pi b$. For instance, consider Example 2,

$$\Pi J = \begin{bmatrix} J_{11} & J_{12} \\ 0 & 0 \end{bmatrix}, \quad \Pi J \Pi = \begin{bmatrix} J_{11} & 0 \\ 0 & 0 \end{bmatrix}.$$

The Euler–Lagrange equation for (P0) has an extra term $J_{12}b_2$ if writing $b = (b_1, b_2)$. This extra term comes from the normal space since only b_1 is used in defining the SDE on the manifold. \square

PROPOSITION 9. *If $a(x) = \sigma^2(x)I$ (scalar matrix) and Π_x is an orthogonal projection $\forall x \in \mathcal{M}$, then (P1) is equivalent to (P*). If $a(x)$ is not a scalar matrix, then (P1) is not equivalent to (P*) in general.*

Proof. If a is a scalar matrix, then Π^{-1} is identity, and $\|\cdot\|_a = \|\cdot\|_{\tilde{a}}$ by Proposition 7, so (P1) is equivalent to (P*).

When a is not a scalar matrix, then in general $\|\cdot\|_a > \|\cdot\|_{\tilde{a}}$ by Proposition 7. So, S^1 is larger than S^M . We shall see that the (constrained) minimizers of these two functionals are also different, i.e., (P1) is not equivalent to (P*). To show this, we continue to consider Example 2 with a state-independent $a(x) \equiv a \forall x$. Since here Π is independent of x , then the Euler–Lagrange equations for (P1) and (P*) are, respectively,

$$\Pi \left(a^{-1}\ddot{\phi}_1 - (a^{-1}\Pi J - J^\top \Pi a^{-1})\dot{\phi}_1 - J^\top \Pi a^{-1}\Pi b(\phi_1) \right) = 0 \tag{P1},$$

$$\tilde{a}^{-1}\ddot{\phi}_* - (\tilde{a}^{-1}\Pi J - J^\top \Pi \tilde{a}^{-1})\dot{\phi}_* - J^\top \Pi \tilde{a}^{-1}\Pi b(\phi_*) = 0 \tag{P*},$$

Using the notation in Example 2 where $a = \begin{bmatrix} A_{11} & A_{12} \\ A_{12}^\top & A_{22} \end{bmatrix}$, and writing $a^{-1} = \begin{bmatrix} B_{11} & B_{12} \\ B_{12}^\top & B_{22} \end{bmatrix}$ and $J = \begin{bmatrix} J_{11} & J_{12} \\ J_{12}^\top & J_{22} \end{bmatrix}$, where B_{11} , J_{11} are both of size $(n-1) \times (n-1)$, and $b = (b_1, b_2)$, $\phi_1 = (\phi_{11}, \phi_{12})$, $\phi_* = (\phi_{*1}, \phi_{*2})$, we can further calculate the above Euler–Lagrange equations for (P1) and (P*) as

$$B_{11}\ddot{\phi}_{11} - (B_{11}J_{11} - J_{11}^\top B_{11})\dot{\phi}_{11} - J_{11}^\top B_{11}b_1(\phi) = 0 \tag{P1},$$

$$A_{11}^{-1}\ddot{\phi}_{*1} - (A_{11}^{-1}J_{11} - J_{11}^\top A_{11}^{-1})\dot{\phi}_{*1} - J_{11}^\top A_{11}^{-1}b_1(\phi_*) = 0 \tag{P*}.$$

The Euler–Lagrange equation for (P*) only involves A_{11}^{-1} , i.e., \tilde{a} ; thus it defines a boundary value problem of the second-order differential equation intrinsically on the plane \mathcal{M} . The Euler–Lagrange equation for (P1) involves a^{-1} , which includes A_{12} and A_{22} . It is only when $A_{12} = 0$ can we have $A_{11}^{-1} = B_{11}$, and it follows that (P*) is equivalent to (P1). However, in general, the diffusion tensor a cannot guarantee A_{11}^{-1} is equal to B_{11} ; therefore (P*) is not equivalent to (P1). \square

Remark 3. Given $\tilde{a}(x)$, there are various ways to design an augmented $a(x)$ to satisfy the consistence condition $\tilde{a} = \Pi a \Pi^\top$. By Proposition 7, the condition such that

(P1) \iff (P*) for a general Riemannian manifold \mathcal{M} is the following orthogonality condition under the a -metric:

$$(C.10) \quad \langle v, \xi \rangle_a = 0 \quad \forall v \in \text{Img}(\Pi), \quad \xi \in \text{Ker}(\Pi).$$

When $\Pi = \Pi^\top$, this condition means that $\text{Img}(\Pi)$ or $\text{Ker}(\Pi)$ is an invariant subspace of the matrix a^{-1} .

Remark 4. If we consider the following gradient system on a manifold in which $a(x) \equiv I$, $b(x) = -\nabla V(x)$, $\tilde{b} = -\Pi_x \nabla V(x)$, and assume that $\Pi = \Pi^\top$, then we can simplify the Euler–Lagrange equation for (P*) (or equivalently (P1) since $a(x) = I$ here) by noting the fact that $\langle w\tilde{J}v \rangle = \langle v\tilde{J}w \rangle$ holds for any $v, w \in \text{Img}(\Pi)$ (note $\tilde{J} = \nabla \tilde{b}$), i.e., $\Pi(\tilde{J}^\top - \tilde{J})v = 0$. The resulting Euler–Lagrange equation is as follows:

$$\Pi \left(\ddot{\phi} + (\tilde{J}^\top - \tilde{J})\dot{\phi} - \tilde{J}^\top \Pi b(\phi) \right) = \Pi \left(\ddot{\phi} - \tilde{J}^\top \Pi b(\phi) \right) = 0.$$

It is easy to verify that if $\dot{\phi} = \pm \Pi b(\phi)$, then $\ddot{\phi} = \pm \tilde{J}(\phi)\dot{\phi} = \tilde{J}(\phi)\Pi b(\phi)$, and the above Euler–Lagrange equation holds. This justifies, from the large deviation for this special gradient system, the constrained string method in [6] which geometrically solves $\dot{\phi} = \pm \Pi b(\phi)$.

Acknowledgments. We thank the anonymous referees for valuable suggestion.

REFERENCES

- [1] P. BALDI AND L. CARAMELLINO, *General Freidlin–Wentzell large deviations and positive diffusions*, Statist. Probab. Lett., 81 (2011), pp. 1218–1229.
- [2] R. L. BISHOP AND S. I. GOLDBERG, *Tensor Analysis on Manifolds*, Dover Publications, New York, 1980.
- [3] A. CHIARINI AND M. FISCHER, *On large deviations for small noise Ito processes*, Adv. Appl. Probab., 46 (2014), pp. 1126–1147.
- [4] G. CICCOTTI, T. LELIEVRE, AND E. VANDEN-EIJNDEN, *Projection of diffusions on submanifolds: Application to mean force computation*, Comm. Pure Appl. Math., 61 (2008), pp. 371–408.
- [5] P. S. DOYLE AND E. S. G. SHAQFEH, *Dynamic simulation of freely-draining, flexible bead-rod chains: Start-up of extensional and shear flow*, J. Non-Newtonian Fluid Mech., 76 (1998), pp. 43–78.
- [6] Q. DU AND L. ZHANG, *A constrained string method and its numerical analysis*, Commun. Math. Sci., 7 (2009), pp. 1039–1051.
- [7] W. E, W. REN, AND E. VANDEN-EIJNDEN, *String method for the study of rare events*, Phys. Rev. B, 66 (2002), 052301.
- [8] W. E, W. REN, AND E. VANDEN-EIJNDEN, *Minimum action method for the study of rare events*, Comm. Pure Appl. Math., 57 (2004), pp. 637–656.
- [9] M. I. FREIDLIN AND A. D. WENTZELL, *Random Perturbations of Dynamical Systems*, 2nd ed., Springer-Verlag, New York, 1998.
- [10] M. HEYMANN AND E. VANDEN-EIJNDEN, *The geometric minimum action method: A least action principle on the space of curves*, Comm. Pure Appl. Math., 61 (2008), pp. 1052–1117.
- [11] E. P. HSU, *Brownian bridges on Riemannian manifolds*, Probab. Theory Related Fields, 84 (1990), pp. 103–118.
- [12] E. P. HSU, *Stochastic Analysis on Manifolds*, AMS, Providence, RI, 2002.
- [13] H. A. KRAMERS, *Brownian motion in a field of force and the diffusion model of chemical reactions*, Physica, 7 (1940), pp. 284–304.
- [14] L. D. LANDAU AND E. M. LIFSHITZ, *Mechanics*, 3rd ed., Course of Theoretical Physics, Butterworth-Heinemann, London, 1976.
- [15] T. LI, P. ZHANG, AND W. ZHANG, *Nucleation rate calculations for the phase transition of diblock copolymers under stochastic Cahn–Hilliard dynamics*, Multiscale Model. Simul., 11 (2013), pp. 385–409.
- [16] T. LI, P. ZHANG, AND X. ZHOU, *Analysis of 1 + 1 dimensional stochastic models of liquid crystal polymer flows*, Commun. Math. Sci., 2 (2004), pp. 295–316.

- [17] R. S. MAIER AND D. L. STEIN, *Escape problem for irreversible systems*, Phys. Rev. E, 48 (1993), pp. 931–938.
- [18] J. NOCEDAL, *Numerical Optimization*, Springer Ser. Oper. Res., Springer-Verlag, New York, 1999.
- [19] H. C. ÖTTINGER, *Stochastic Processes in Polymeric Fluids: Tools and Examples for Developing Simulation Algorithms*, Springer-Verlag, Berlin, 1996.
- [20] A. PUHALSKII, *On some degenerate large deviation problems*, Electron. J. Probab., 9 (2004), pp. 862–886.
- [21] E. VANDEN-ELJNDEN AND M. HEYMANN, *The geometric minimum action method for computing minimum energy paths*, J. Chem. Phys., 128 (2008), 061103.
- [22] X. WAN, *An adaptive high-order minimum action method*, J. Comput. Phys., 230 (2011), pp. 8669–8682.
- [23] X. WAN, X. ZHOU, AND W. E, *Study of noise-induced transition and the exploration of the configuration space for the Kuramoto-Sivachinsky equation using the minimum action method*, Nonlinearity, 23 (2010), pp. 475–493.
- [24] W. ZHANG, T. LI, AND P. ZHANG, *Numerical study for the nucleation of one-dimensional stochastic Cahn-Hilliard dynamics*, Commun. Math. Sci., 10 (2012), pp. 1105–1132.
- [25] X. ZHOU, W. REN, AND W. E, *Adaptive minimum action method for the study of rare events*, J. Chem. Phys., 128 (2008), 104111.